New Journal of Physics
The open access journal for physics

Theory of resonance shifts of whispering gallery modes by arbitrary plasmonic nanoparticles

Matthew R Foreman[1] **and Frank Vollmer**
Max Planck Institute for the Science of Light, Laboratory of Nanophotonics and Biosensing, Günther-Scharowsky-Straße 1, D-91058 Erlangen, Germany
E-mail: matthew.foreman@mpl.mpg.de

New Journal of Physics **15** (2013) 083006 (27pp)
Received 3 April 2013
Published 2 August 2013
Online at http://www.njp.org/
doi:10.1088/1367-2630/15/8/083006

Abstract. Shifts of the resonance frequency of high Q whispering gallery modes (WGMs) in spherical dielectric microresonators by plasmonic nanoparticles can be greater than the WGM line width, such that the perturbation theory commonly used for describing resonance shifts by dielectric nanoparticles (Teraoka and Arnold 2006 *J. Opt. Soc. Am.* B **23** 1381) is no longer applicable. This paper therefore reports on an analytic framework, based on generalized Lorenz–Mie theory, capable of describing resonance shifts by metallic nanoparticles supporting plasmon oscillations. Generalization to nanoparticles of arbitrary geometry is presented by employing the extended boundary condition method. Within this framework, hybrid resonance conditions for coupled spherical photonic and plasmonic resonators are established and shown to simplify for small plasmonic nanoparticles. Approximate analytic formulae are derived for the shift and broadening of the isolated WGM and plasmon resonances, from which either apparent resonance shifts or mode splitting are shown to follow. Tuning of plasmon resonances using, for example, core–shell nanoparticles to attain a large spectral overlap between WGM and plasmon resonances is demonstrated to significantly enhance the magnitude of resonance shifts, with a 60-fold enhancement achieved without any optimization. Hybridization of photonic–plasmonic resonances is furthermore demonstrated

[1] Author to whom any correspondence should be addressed.

(in addition to hybridization of transverse electric–transverse magnetic WGMs) and the associated level repulsion illustrated. Finally, the dependence of WGM resonance shifts on the orientation of silver nanorods is theoretically investigated and found to be strong by virtue of the asymmetry of the nanorod.

Contents

1. Introduction

The field of nanoplasmonics is undoubtedly one that has attracted much research effort in recent years, and has seen successful results in a wide array of applications, such as single molecule spectroscopy, improved drug delivery, light harvesting, integrated circuits and much more [1, 2]. Whilst the motivation for exploitation of plasmonic structures varies between applications, their popularity typically derives from the ability to strongly localize an optical field and the ability to modify, control and optimize the resonant nature of coupling between light and electrons [3]. Within this rapidly developing and multidisciplinary science, one research direction that has emerged, for example, is the use of plasmon resonances for both chemical and biological sensing purposes [4]. Phenomenologically, plasmonic sensors rely on the sensitivity of the resonance frequency of either surface [5, 6] or localized plasmons [7] excited in metallic structures, to the properties of the local environment, such as refractive index. For example, when a (large) molecule is in close proximity to a surface plasmon sensor, the effective optical path length travelled by a resonant surface mode is increased, resulting in a shift in the resonance frequency, which can be detected by monitoring the transmission properties of a swept laser or broadband source [8].

Ohmic losses in metals, however, imply that plasmons are short lived and consequently plasmon resonances are broad. Low Q factors ($\sim$100) inherent in plasmonic sensing hence limit sensitivity levels achievable, making them unsuitable for applications demanding single, or few, molecule sensitivity, such as early pathogen/toxin detection. Dielectric whispering gallery mode resonators (WGMRs), however, represent a similar sensing technology, whereby it is

the sensitivity of optical resonances in dielectric cavities, e.g. a microsphere, that is exploited to probe the local surroundings [9]. Since dielectric materials exhibit far lower absorption than metals, high Q resonances can be supported (ultimately limited to $\sim 10^{10}$ [10]), and thus sensitivity levels are intrinsically higher, allowing detection down to the single virus level [11].

Traditionally, shifts in resonance frequencies are analysed using, what has become known as, the reactive sensing principle [12], which derives from a first order perturbation treatment of electromagnetic scattering, originally derived in the microwave domain [13, 14], but later extended into the optical regime by Arnold and co-workers [15–17]. Specifically, the reactive sensing principle states that the spectral position of a whispering gallery mode (WGM) resonance is shifted when a nanoparticle (NP) enters the evanescent field of a WGMR by an amount inversely proportional to the energy in the WGMR and proportional to the local intensity seen by the NP and the polarizability of the NP (cf equation (25) below). Combination of high Q dielectric WGMRs and plasmonic NPs, therefore represents a means by which the detection envelope can be pushed further. Two alternative approaches are, indeed, currently being actively pursued in this vein, namely exploitation of local field enhancements, or plasmonic hotspots [18–22] and use of NPs as analyte labels [23–25], whereby sensitivity gains follow by virtue of the increased near field or NP polarizability respectively.

Despite the widespread success of the reactive sensing principle, its validity is known to be restricted to scenarios in which resonance shifts are less than half the line width of the WGM [26]. Use of plasmonic NPs to increase the magnitude of resonance shifts can therefore necessitate the use of an alternative theory since resonance shifts can be greatly amplified. To illustrate this point consider a typical WGM resonance with a Q factor 10^6 or 10^5, i.e. a spectral width on the order of 1–10 pm. Theoretically, it has been shown [20] that adsorption of an individual MS2 virus gives rise to a resonance shift of approximately 0.25 fm (or equivalently 0.25×10^{-3}–0.25×10^{-4} line widths respectively), yet near field intensity enhancements as high as 10^5 have been reported in the literature [27]. Shifts greater than resonance line widths are hence entirely plausible, if not expected, in NP based optical WGM sensing. Ultra-high Q resonances have, similarly, been shown to undergo mode splitting upon interaction with small dielectric scatterers [28, 29], which cannot be described using the reactive sensing principle. Conditions for observing mode splitting with metal-based NPs are, moreover, less stringent than for dielectric NPs because they (a) have a larger off-resonance polarizability in the optical regime, and (b) can support collective electron excitations, i.e. plasmons, leading to enhanced coupling. It should also be noted that with increasing coupling strength comes increased scattering losses, in turn implying broadening of WGM resonances. Again the need for an alternative description is evident, since these feature are not accounted for by the reactive sensing principle.

With these points in mind, this paper aims to present an analytic framework, within which the perturbation of WGMRs by arbitrary plasmonic NPs can be described. Section 2 presents the fundamental scattering formalism used to do so. The work described therein extends earlier literature which considered perturbations to WGMRs from spherical dielectric Rayleigh scatterers by employing generalized Lorenz–Mie theory [29]. Here, however, scattering from larger particle sizes is considered, with simplifications for smaller NPs given later. Metallic NPs can also be fully described within the scattering framework given here, such that resulting formulae embody plasmonic effects. Application of Waterman's extended boundary condition method [30], furthermore, allows arbitrary NP geometries, such as core–shells, nanorods and nanocubes, to be described. Section 3 proceeds to derive hybrid photonic–plasmonic resonance

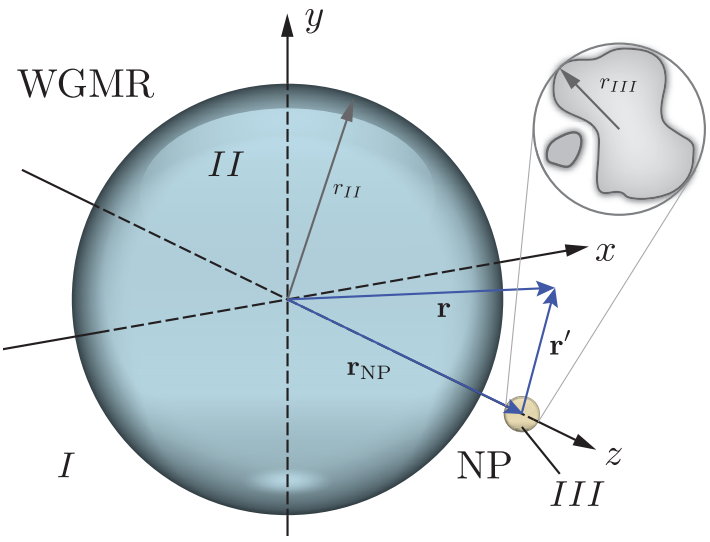

Figure 1. Geometry and coordinate systems used in the coupling calculations.

conditions for the WGMR-NP system. Naturally, the formulae obtained are more involved than those derived from the reactive sensing principle, however this reflects the richer physics which they express. Nevertheless, simplifications are sought to aid ease of use, with approximate solutions presented in concert to exact results. Section 4 briefly describes an approximate means by which the extinction spectrum of the hybrid resonant system can be determined, without the need to solve the full scattering problem, before numerical results are given in section 5. In view of the wealth of physical effects that stem from the coupled resonator system, such as mode hybridization and resonance splitting, section 5 attempts to give a brief survey of NP geometries from which they can arise. Accordingly, after initial model verification using homogeneous dielectric spherical NPs, results are presented for metallic spheres, resonant core–shell NPs and nanorods. Discussion of the results is given in section 6. With the aim of facilitating practical implementation of the theory, a number of supplementary appendices are also given elaborating a number of finer mathematical details.

2. Formulation of the problem

In this paper the resonance shift of WGMs within a spherical WGMR due to the presence of an arbitrary NP will be considered. Attention will initially be restricted to spherical NPs, however extension to composite NPs, such as core–shell NPs, and more complex geometries, such as nanorods, will subsequently be given. Figure 1 depicts the system geometry under consideration, whereby three distinct regions, labelled I, II and III, can be seen. Initially, restricting to spherical NPs, regions II and III define the volume of the WGMR and NP respectively, whilst I denotes the medium within which they are immersed. Employing generalized Lorenz–Mie theory [31], the electric field within each of these regions can thus be represented as a superposition of multipole (or Mie) modes, $\mathbf{E}_{lm}^{\nu(j)}(\mathbf{r})$, viz:

$$\mathbf{E}^{\mathrm{I}}(\mathbf{r}) = \sum_{\nu,lm} a_{lm}^{\nu}\mathbf{E}_{lm}^{\nu(3)}(\mathbf{r}) + b_{lm}^{\nu}\mathbf{E}_{lm}^{\nu(1)}(\mathbf{r}) + \tilde{d}_{lm}^{\nu}\mathbf{E}_{lm}^{\nu(1)}(\mathbf{r}-\mathbf{r}_{\mathrm{NP}}), \tag{1a}$$

$$\mathbf{E}^{\mathrm{II}}(\mathbf{r}) = \sum_{\nu,lm} c^{\nu}_{lm}\mathbf{E}^{\nu(3)}_{lm}(\mathbf{r}), \tag{1b}$$

$$\mathbf{E}^{\mathrm{III}}(\mathbf{r}) = \sum_{\nu,lm} \tilde{f}^{\nu}_{lm}\mathbf{E}^{\nu(3)}_{lm}(\mathbf{r}-\mathbf{r}_{\mathrm{NP}}). \tag{1c}$$

Explicit expressions for the Mie modes are given in appendix A, however here it is noted that each Mie mode is indexed by the polar and azimuthal numbers $l = 1, 2, \ldots,$ and $m = -l, -l+1, \ldots, l$. ν denotes either electric ($\mathbf{E}$) or magnetic (m) Mie modes (also commonly referred to as transverse magnetic (TM) and transverse electric (TE) respectively). Physically, the $j = 1$ modes represent multipole sources, in which energy flows outward from $\mathbf{r} = \mathbf{0}$ whilst $j = 2$ represents field sinks with energy flowing inwards towards the sink position. In contrast, $j = 3$ modes constitute a superposition of both $j = 1$ and 2 in equal measure such that they have finite energy density at the origin. Accordingly, the expansion coefficients a^{ν}_{lm}, b^{ν}_{lm}, c^{ν}_{lm}, $\tilde{d}^{\nu}_{lm}$ and $\tilde{f}^{\nu}_{lm}$ represent the illumination field, the field scattered from the WGMR, the field within the WGMR, the field scattered from the NP and the field within the NP respectively.

Imposing continuity of the tangential field components at the surface of the WGMR and NP allows the expansion coefficients to be analytically related, however it should be noted from equations (1) that the expansions of the field scattered from, and generated within, the NP are performed in a coordinate system with origin at $\mathbf{r} = \mathbf{r}_{\mathrm{NP}}$, i.e. the centre of the NP (as denoted by the tilde notation). Matching of the fields, therefore, is most easily accomplished if the shift formulae, equations (B.2), are used to express all modes in the same coordinate system, which leads to the continuity equations:

$$\left[a^{\nu}_{lm} + d^{\nu}_{lm}\right]\psi^{(3)}_{l}(k^{\mathrm{I}}r_{\mathrm{II}}) + b^{\nu}_{lm}\psi^{(1)}_{l}(k^{\mathrm{I}}r_{\mathrm{II}}) = c^{\nu}_{lm}\psi^{(3)}_{l}(k^{\mathrm{II}}r_{\mathrm{II}}), \tag{2a}$$

$$\left[\tilde{a}^{\nu}_{lm} + \tilde{b}^{\nu}_{lm}\right]\psi^{(3)}_{l}(k^{\mathrm{I}}r_{\mathrm{III}}) + \tilde{d}^{\nu}_{lm}\psi^{(1)}_{l}(k^{\mathrm{I}}r_{\mathrm{III}}) = \tilde{f}^{\nu}_{lm}\psi^{(3)}_{l}(k^{\mathrm{III}}r_{\mathrm{III}}), \tag{2b}$$

$$k^{\mathrm{I}}_{s}\left[a^{\nu}_{lm} + d^{\nu}_{lm}\right]h^{(3)}_{l}(k^{\mathrm{I}}r_{\mathrm{II}}) + b^{\nu}_{lm}h^{(1)}_{l}(k^{\mathrm{I}}r_{\mathrm{II}}) = k^{\mathrm{II}}_{s}c^{\nu}_{lm}h^{(3)}_{l}(k^{\mathrm{II}}r_{\mathrm{II}}), \tag{2c}$$

$$k^{\mathrm{I}}_{s}\left[\tilde{a}^{\nu}_{lm} + \tilde{b}^{\nu}_{lm}\right]h^{(3)}_{l}(k^{\mathrm{I}}r_{\mathrm{III}}) + \tilde{d}^{\nu}_{lm}h^{(1)}_{l}(k^{\mathrm{I}}r_{\mathrm{III}}) = k^{\mathrm{III}}_{s}\tilde{f}^{\nu}_{lm}h^{(3)}_{l}(k^{\mathrm{III}}r_{\mathrm{III}}), \tag{2d}$$

where $\psi^{(j)}_{l}(z) = \partial[zh^{(j)}_{l}(z)]/\partial z$ and $s = 1, 2$ for $\nu = E, M$ respectively.

WGMRs are commonly excited by means of a tapered fibre or prism [32], such that the illumination field is only significant over a small region of space near one side of the WGMR. As such it is reasonable to neglect the $\tilde{a}^{\nu}_{lm}$ terms in both equations (2*b*) and (2*d*), which describe the illumination field near the NP. Following standard algebraic manipulation, equations (2*a*)–(2*d*) yield the scaling relations:

$$b^{\nu}_{lm} = \eta^{\nu}_{l}(k^{\mathrm{I}}, k^{\mathrm{II}}, r_{\mathrm{II}})\left[a^{\nu}_{lm} + d^{\nu}_{lm}\right], \tag{3a}$$

$$c^{\nu}_{lm} = \zeta^{\nu}_{l}(k^{\mathrm{I}}, k^{\mathrm{II}}, r_{\mathrm{II}})\left[a^{\nu}_{lm} + d^{\nu}_{lm}\right], \tag{3b}$$

$$\tilde{d}^{\nu}_{lm} = \eta^{\nu}_{l}(k^{\mathrm{I}}, k^{\mathrm{III}}, r_{\mathrm{III}})\,\tilde{b}^{\nu}_{lm}, \tag{3c}$$

$$\tilde{f}^{\nu}_{lm} = \zeta^{\nu}_{l}(k^{\mathrm{I}}, k^{\mathrm{III}}, r_{\mathrm{III}})\,\tilde{b}^{\nu}_{lm}, \tag{3d}$$

where

$$\eta_l^{\nu}(k^i, k^j, \rho) = \frac{k_s^i h_l^{(3)}(k^i\rho)\psi_l^{(3)}(k^j\rho) - k_s^j h_l^{(3)}(k^j\rho)\psi_l^{(3)}(k^i\rho)}{k_s^j h_l^{(3)}(k^j\rho)\psi_l^{(1)}(k^i\rho) - k_s^i h_l^{(1)}(k^i\rho)\psi_l^{(3)}(k^j\rho)}, \tag{4a}$$

$$\zeta_l^{\nu}(k^i, k^j, \rho) = \frac{k_s^i h_l^{(3)}(k^i\rho)\psi_l^{(1)}(k^i\rho) - k_s^i h_l^{(1)}(k^i\rho)\psi_l^{(3)}(k^i\rho)}{k_s^j h_l^{(3)}(k^j\rho)\psi_l^{(1)}(k^i\rho) - k_s^i h_l^{(1)}(k^i\rho)\psi_l^{(3)}(k^j\rho)}. \tag{4b}$$

Henceforth, the notation $\eta_l^{\nu,1} = \eta_l^{\nu}(k^{\mathrm{I}}, k^{\mathrm{II}}, r_{\mathrm{II}})$ and $\eta_l^{\nu,2} = \eta_l^{\nu}(k^{\mathrm{I}}, k^{\mathrm{III}}, r_{\mathrm{III}})$ (and similarly for $\zeta_l^{\nu,i}$) will be used, for simplicity. For later convenience the scaling coefficient $\gamma_l^{\nu,i} = \eta_l^{\nu,i}/\zeta_l^{\nu,i}$ is also defined here.

To reduce the system of equations defined by equations (3), the shift formulae (equation (B.3)) must be invoked. Generally, however, equations (B.3) are seen to couple modes of different azimuthal numbers m. Cylindrical symmetry inherent in figure 1, however, suggests that judicious choice of the coordinate axes can avoid such a mathematical complication. Indeed, a polar axis chosen to lie along the line joining the WGMR and NP centres, represents a convenient quantization axis in which coupling between azimuthal modes is avoided [33]. Each azimuthal mode number m hence defines an independent system of equations (as per equations (3)), which can subsequently be further manipulated so as to eliminate the coefficients d_{lm}^{ν}, and f_{lm}^{ν} (and their shifted counterparts). Written in matrix form, the resulting coefficients obey the relation

$$(\mathbb{I} - \mathbb{A}\mathbb{\Gamma}_m)\begin{bmatrix}\mathbf{b}_m^E\\ \mathbf{b}_m^M\\ \mathbf{c}_m^E\\ \mathbf{c}_m^M\end{bmatrix} = \begin{bmatrix}\mathbb{N}_m^{E,1} & \mathbb{0}\\ \mathbb{0} & \mathbb{N}_m^{M,1}\\ \mathbb{Z}_m^{E,1} & \mathbb{0}\\ \mathbb{0} & \mathbb{Z}_m^{M,1}\end{bmatrix}\begin{bmatrix}\mathbf{a}_m^E\\ \mathbf{a}_m^M\end{bmatrix}, \tag{5}$$

where $\mathbf{a}_m^{\nu}$ denotes the vector formed by stacking the coefficients a_{lm}^{ν} for $l = |m|, |m|+1, \ldots$ (and similarly for $\mathbf{b}_m^{\nu}$ and $\mathbf{c}_m^{\nu}$),

$$\mathbb{A}\mathbb{\Gamma}_m = \begin{bmatrix}\mathbb{N}_m^{E,1}\mathbb{\Delta}_{m,1} & \mathbb{N}_m^{E,1}\mathbb{\Delta}_{m,3} & \mathbb{0} & \mathbb{0}\\ \mathbb{N}_m^{M,1}\mathbb{\Delta}_{m,4} & \mathbb{N}_m^{M,1}\mathbb{\Delta}_{m,2} & \mathbb{0} & \mathbb{0}\\ \mathbb{0} & \mathbb{0} & \mathbb{Z}_m^{E,1}\mathbb{\Delta}_{m,1}\mathbb{G}_m^{E,1} & \mathbb{Z}_m^{E,1}\mathbb{\Delta}_{m,3}\mathbb{G}_m^{M,1}\\ \mathbb{0} & \mathbb{0} & \mathbb{Z}_m^{M,1}\mathbb{\Delta}_{m,4}\mathbb{G}_m^{E,1} & \mathbb{Z}_m^{M,1}\mathbb{\Delta}_{m,2}\mathbb{G}_m^{M,1}\end{bmatrix}. \tag{6}$$

$\mathbb{I}$ is the identity matrix, $\mathbb{0}$ is a matrix of zeros, $\mathbb{N}_m^{\nu,i}$, $\mathbb{Z}_m^{\nu,i}$ and $\mathbb{G}_m^{\nu,i}$ are diagonal matrices with diagonal elements $\eta_l^{\nu,i}$, $\zeta_l^{\nu,i}$ and $\gamma_l^{\nu,i}$, respectively, and

$$\mathbb{\Delta}_{m,1} = \tilde{\mathbb{A}}_m^{(1)}\mathbb{N}_m^{E,2}\mathbb{A}_m^{(1)} + \tilde{\mathbb{B}}_m^{(1)}\mathbb{N}_m^{M,2}\mathbb{B}_m^{(1)}, \tag{7a}$$

$$\mathbb{\Delta}_{m,2} = \tilde{\mathbb{A}}_m^{(1)}\mathbb{N}_m^{M,2}\mathbb{A}_m^{(1)} + \tilde{\mathbb{B}}_m^{(1)}\mathbb{N}_m^{E,2}\mathbb{B}_m^{(1)}, \tag{7b}$$

$$\mathbb{\Delta}_{m,3} = \frac{k_2^{\mathrm{I}}}{k^{\mathrm{I}}}\left(\tilde{\mathbb{A}}_m^{(1)}\mathbb{N}_m^{E,2}\mathbb{B}_m^{(1)} + \tilde{\mathbb{B}}_m^{(1)}\mathbb{N}_m^{M,2}\mathbb{A}_m^{(1)}\right), \tag{7c}$$

$$\mathbb{\Delta}_{m,4} = \frac{k^{\mathrm{I}}}{k_2^{\mathrm{I}}}\left(\tilde{\mathbb{A}}_m^{(1)}\mathbb{N}_m^{M,2}\mathbb{B}_m^{(1)} + \tilde{\mathbb{B}}_m^{(1)}\mathbb{N}_m^{E,2}\mathbb{A}_m^{(1)}\right). \tag{7d}$$

Table 1. Parameter values for equation (9).

j	ν ($\bar{\nu}$)	μ ($\bar{\mu}$)	S_j^{AB}	S_j^{BA}	S_j^{BB}
1	E (M)	M (E)	$k^{\mathrm{I}}/k_2^{\mathrm{I}}$	$k_2^{\mathrm{I}}/k^{\mathrm{I}}$	1
2	M (E)	E (M)	$k_2^{\mathrm{I}}/k^{\mathrm{I}}$	$k^{\mathrm{I}}/k_2^{\mathrm{I}}$	1
3	E (M)	M (E)	$k_2^{\mathrm{I}}/k^{\mathrm{I}}$	$k_2^{\mathrm{I}}/k^{\mathrm{I}}$	$(k_2^{\mathrm{I}}/k^{\mathrm{I}})^2$
4	M (E)	E (M)	$k^{\mathrm{I}}/k_2^{\mathrm{I}}$	$k^{\mathrm{I}}/k_2^{\mathrm{I}}$	$(k^{\mathrm{I}}/k_2^{\mathrm{I}})^2$

The matrices $\mathbb{A}_m^{(1)}$ and $\mathbb{B}_m^{(1)}$ are full matrices with elements given by (with a slight abuse of notation) $\mathcal{A}_{Lm}^{lm} = \mathcal{A}_{Lm}^{lm(1)}(\mathbf{r}_{\mathrm{NP}})$ and $\mathcal{B}_{Lm}^{lm} = \mathcal{B}_{Lm}^{lm(1)}(\mathbf{r}_{\mathrm{NP}})$ (see appendix B). Similarly $\tilde{\mathbb{A}}_m^{(1)}$ and $\tilde{\mathbb{B}}_m^{(1)}$ describe shifts in the opposite direction and are thus formed from the elements $\tilde{\mathcal{A}}_{Lm}^{lm} = \mathcal{A}_{Lm}^{lm(1)}(-\mathbf{r}_{\mathrm{NP}})$ and $\tilde{\mathcal{B}}_{Lm}^{lm} = \mathcal{B}_{Lm}^{lm(1)}(-\mathbf{r}_{\mathrm{NP}})$.

Extension of the presented scattering formalism to consider non-spherical NPs can be achieved with recourse to the extended boundary condition method originally proposed by Waterman [30, 34]. In this paradigm, region III no longer defines the volume of a spherical NP, but instead is defined by a fictitious spherical surface circumscribing an arbitrarily shaped, finite NP (see figure 1). The incident field and the field 'scattered' from this fictitious surface is once again represented as a superposition of Mie modes. Expansion coefficients of the incident and scattered fields are then related by the so-called T-matrix of the NP, such that in the derivations above equation (3*c*) becomes

$$\begin{bmatrix} \tilde{\mathbf{d}}^E \\ \tilde{\mathbf{d}}^M \end{bmatrix} = \begin{bmatrix} \mathbb{T}^{EE} & \mathbb{T}^{EM} \\ \mathbb{T}^{ME} & \mathbb{T}^{MM} \end{bmatrix} \begin{bmatrix} \tilde{\mathbf{b}}^E \\ \tilde{\mathbf{b}}^M \end{bmatrix}. \tag{8}$$

An analogous equation, for the $\tilde{f}_{lm}^{\nu}$ coefficients (albeit now only valid within the NP volume and not the entirety of region III) can also be written in terms of a Q-matrix [35], however this is not required for the present derivations and is hence omitted. The elements of the T-matrix can be found, by performing surface integrals of cross products of different combinations of Mie modes over the surface of the NP (see [35] for full details), for which efficient and accurate routines already exist. For absorbing materials, such as metals, care must be taken with the algorithmic details by which the T-matrix is calculated [36]. In general, it is important to note that equation (8) is not separable in m unless the NP is axial symmetric about the polar axis (e.g. a circular cylinder). Accordingly, $\tilde{\mathbf{b}}^{\nu}$ denotes the vector formed by stacking the coefficients $\tilde{b}_{lm}^{\nu}$ for all (l, m) (and similarly for $\tilde{\mathbf{d}}^{\nu}$). Consequently, the equivalent system matrix $\mathbb{I} - \mathbb{A}\mathbb{\Gamma}$ is also no longer block diagonal in general and hence the m subscript must be dropped. Formally, however, the electromagnetic scattering problem may still be expressed in the same form as equations (5) and (6) (with omission of the m subscript), except now

$$\mathbb{A}_j = \tilde{\mathbb{A}}^{(1)}\mathbb{T}^{\nu\mu}\mathbb{A}^{(1)} + S_j^{AB}\tilde{\mathbb{A}}^{(1)}\mathbb{T}^{\nu\bar{\mu}}\mathbb{B}^{(1)} + S_j^{BA}\tilde{\mathbb{B}}^{(1)}\mathbb{T}^{\bar{\nu}\mu}\mathbb{A}^{(1)} + S_j^{BB}\tilde{\mathbb{B}}^{(1)}\mathbb{T}^{\bar{\nu}\bar{\mu}}\mathbb{B}^{(1)}, \tag{9}$$

where the appropriate values of ν, μ and S_j are shown in table 1. The bar notation on ν and μ implies the complimentary mode index (see table 1).

3. Resonance conditions

Resonances in an isolated WGMR follow from equation (5) by setting $\mathbb{\Delta\Gamma} = 0$ (i.e. dropping the perturbation of the NP) and looking for complex poles in the matrices $\mathbb{N}_m^{\nu,1}$ and $\mathbb{Z}_m^{\nu,1}$. The real and imaginary parts of these roots determine the resonance wavelengths and line width respectively. Since Mie resonances for a single sphere are well known and described in many texts [37, 38] they will not be considered further here, however it is noted that the poles of both $\mathbb{N}_m^{\nu,1}$ and $\mathbb{Z}_m^{\nu,1}$ occur at the same wavelengths (for a fixed resonator size). Coupling between the NP and WGMR, however, alters the resonance condition as described by the perturbing matrix $\mathbb{\Delta\Gamma}$. Optical resonances for the combined WGMR-NP system, can thus be found by determination of the roots $|\mathbb{I} - \mathbb{\Delta\Gamma}| = 0$. Given that $\mathbb{\Delta\Gamma}$ is block diagonal the determinant $|\mathbb{I} - \mathbb{\Delta\Gamma}|$ can be written as the product of the determinants of the upper diagonal block and lower diagonal block. The poles of these blocks, again occur at the same wavelengths (for fixed r_{II}), such that it is sufficient to consider the resonance condition $|\mathbb{I} - \mathbb{\Delta\Lambda}| = 0$, where

$$\mathbb{\Delta\Lambda} = \begin{bmatrix} \mathbb{N}^{E,1}\mathbb{\Delta}_1 & \mathbb{N}^{E,1}\mathbb{\Delta}_3 \\ \mathbb{N}^{M,1}\mathbb{\Delta}_4 & \mathbb{N}^{M,1}\mathbb{\Delta}_2 \end{bmatrix}. \tag{10}$$

For axially symmetric NPs, $\mathbb{\Delta\Lambda}$ is furthermore block diagonal in m, such that determination of the resonances is computationally easier. Resonance conditions can, however, equivalently be expressed via the condition $\alpha_{lm}^k = 0$, where α_{lm}^k are the eigenvalues of $\mathbb{I} - \mathbb{\Delta\Lambda}$. It should be noted that for each mode index (l, m) two eigenvalues can be found, which are indexed by the superscript k. For an isolated WGMR these two eigenvalues correspond to TM and TE resonances. For the combined WGMR-NP system these resonances can be classified as quasi-TM and -TE modes.

Analytic determination of the eigenvalues of $\mathbb{I} - \mathbb{\Delta\Lambda}$ is, in general, intractable, however a number of approximations can be made. As a first order approach, matrix perturbation theory can be applied [39], whereby $\mathbb{\Delta\Lambda}$ is considered as a perturbation to the identity matrix. Noting that all eigenvalues of $\mathbb{I}$ are unity and that the first order perturbations to these eigenvalues are given by the on-diagonal elements of $\mathbb{\Delta\Lambda}$ yields the resonance conditions for the (l, m) quasi-TM ($\nu = E$) and quasi-TE ($\nu = M$) modes as

$$\begin{aligned} 0 = \frac{1}{\eta_l^{\nu,1}} - \sum_{L,L'} \Big[& \tilde{\mathcal{A}}_{Lm}^{lm} T_{LmL'm}^{\nu\nu} \mathcal{A}_{lm}^{L'm} + \tilde{\mathcal{B}}_{Lm}^{lm} T_{LmL'm}^{\bar{\nu}\bar{\nu}} \mathcal{B}_{lm}^{L'm} \\ & + S_s^{AB} \tilde{\mathcal{A}}_{Lm}^{lm} T_{LmL'm}^{\nu\bar{\nu}} \mathcal{B}_{lm}^{L'm} + S_s^{BA} \tilde{\mathcal{B}}_{Lm}^{lm} T_{LmL'm}^{\bar{\nu}\nu} \mathcal{A}_{lm}^{L'm} \Big], \end{aligned} \tag{11}$$

where again $s = 1, 2$ for $\nu = E, M$. Asymptotically, equation (11) should reproduce the resonance condition for a bare WGMR as the NP is moved further from the WGMR. Letting $r_{\mathrm{NP}} \to \infty$ and observing $\mathcal{A}_{Lm}^{lm}$ and $\mathcal{B}_{Lm}^{lm} \to 0$ in this limit allows equations (11) to be written in the form $1/\eta_l^{\nu,1} = 0$, thus confirming physical expectations. When considering spherical NPs, the resonance conditions expressed by equation (11) simplify to

$$0 = \frac{1}{\eta_l^{E,1}} - \sum_{L} \left[\tilde{\mathcal{A}}_{Lm}^{lm} \eta_L^{E,2} \mathcal{A}_{lm}^{Lm} + \tilde{\mathcal{B}}_{Lm}^{lm} \eta_L^{M,2} \mathcal{B}_{lm}^{Lm} \right] \tag{12a}$$

for the quasi-TM mode and

$$0 = \frac{1}{\eta_l^{M,1}} - \sum_L \left[\tilde{\mathcal{A}}_{Lm}^{lm} \eta_L^{M,2} \mathcal{A}_{lm}^{Lm} + \tilde{\mathcal{B}}_{Lm}^{lm} \eta_L^{E,2} \mathcal{B}_{lm}^{Lm} \right] \tag{12b}$$

for the quasi-TE mode.

Assuming the NP to be small (i.e. $k\, r_{\mathrm{III}} \ll 1$) implies that the NP can further be treated as a dipole scatterer, such that only $L = 1$ terms in equation (11) (or equations (12)) need be considered. If the magnetic dipole terms are also negligible then the first order resonance conditions can be written

$$0 = \frac{1}{\eta_l^{E,1} \eta_1^{E,2}} - \tilde{\mathcal{A}}_{1m}^{lm} \mathcal{A}_{lm}^{1m} \quad \text{for quasi-TM modes,} \tag{13a}$$

$$0 = \frac{1}{\eta_l^{M,1} \eta_1^{E,2}} - \tilde{\mathcal{B}}_{1m}^{lm} \mathcal{B}_{lm}^{1m} \quad \text{for quasi-TE modes.} \tag{13b}$$

In this scenario, it is observed that $\mathcal{A}_{lm}^{1m} = \mathcal{B}_{lm}^{1m} = 0$ for $|m| > 1$, such that only the $|m| \leqslant 1$ azimuthal modes experience a shift in resonance frequency from that of an isolated WGMR. Furthermore, it is noted that the $m = 0$ TE modes also do not experience a shift. For high Q WGM resonances, the shifting of the low order ($|m| \leqslant 1$) azimuthal modes relative to the higher order modes can give rise to mode splitting [40]. For lower Q resonances, such as that considered in section 5, a shift of the aggregate spectral line results. This point is further discussed in section 4.

Since $\mathbb{\Delta}\mathbb{\Lambda}$ is a full matrix equations (11)–(13) only describe approximate resonance conditions for the hybrid system. For axially symmetric NPs (e.g. nanorods) aligned such that their symmetry axis lies along the global polar axis, off diagonal elements of the associated T matrix are identically zero and hence the approximation provides accurate results. Naturally, the same holds true for rotational symmetric NPs such as spheres. If, however, the NP possesses no symmetry, or the symmetry axis does not lie along the z-axis the approximation worsens. More exact resonance conditions than those defined by equations (11)–(13) can, fortunately, be found. To do so requires diagonalization of $\mathbb{\Delta}\mathbb{\Lambda}$, which can trivially be achieved numerically, whereby it then follows that $\alpha_{lm}^k = 1 - \beta_{lm}^k$, where β_{lm}^k are the eigenvalues of $\mathbb{\Delta}\mathbb{\Lambda}$. Analytic diagonalization of $\mathbb{\Delta}\mathbb{\Lambda}$ can, however, also allow greater physical insight to be obtained, albeit this requires further approximations to be made. For example, if considering spherical NPs, and if coupling between modes of different l is neglected, the matrices $\mathbb{\Delta}_{m,i}$ become diagonal, such that each block of $\mathbb{\Delta}\mathbb{\Lambda}_m$ is also diagonal. Accordingly it follows that

$$\beta_{lm}^{1,2} = \frac{1}{2} \left(\left[\mathbb{\Delta}_{m,1}\right]_{ll} + \left[\mathbb{\Delta}_{m,2}\right]_{ll} \pm \sqrt{\left(\left[\mathbb{\Delta}_{m,1}\right]_{ll} - \left[\mathbb{\Delta}_{m,2}\right]_{ll}\right)^2 + 4 \left[\mathbb{\Delta}_{m,3}\right]_{ll} \left[\mathbb{\Delta}_{m,4}\right]_{ll}} \right) \tag{14}$$

such that

$$\beta_{lm}^1 \approx \left[\mathbb{\Delta}_{m,1}\right]_{ll} + \frac{\left[\mathbb{\Delta}_{m,3}\right]_{ll} \left[\mathbb{\Delta}_{m,4}\right]_{ll}}{\left[\mathbb{\Delta}_{m,1}\right]_{ll} - \left[\mathbb{\Delta}_{m,2}\right]_{ll}} \tag{15a}$$

and

$$\beta_{lm}^2 \approx \left[\mathbb{\Delta}_{m,2}\right]_{ll} - \frac{\left[\mathbb{\Delta}_{m,3}\right]_{ll} \left[\mathbb{\Delta}_{m,4}\right]_{ll}}{\left[\mathbb{\Delta}_{m,1}\right]_{ll} - \left[\mathbb{\Delta}_{m,2}\right]_{ll}}, \tag{15b}$$

where $[\mathbb{X}]_{ij}$ denotes the (i, j)th element of the matrix $\mathbb{X}$. Whilst previously the eigenvalue pairs for each mode index (l, m) could be attributed to TE and TM polarized modes, no such association can be made for equation (14). Instead, inter-polarization coupling, as determined by the matrices $\mathbb{\Delta}_{m,3}$ and $\mathbb{\Delta}_{m,4}$, gives two hybridized levels with a mixed polarization state. Adopting an electric dipole scattering approximation for the NP, the hybrid resonance conditions are explicitly given by

$$0 = \frac{1}{\eta_l^{E,1}\eta_1^{E,2}} - \tilde{\mathcal{A}}_{1m}^{lm}\mathcal{A}_{lm}^{1m} - \frac{\eta_l^{M,1}\tilde{\mathcal{A}}_{1m}^{lm}\mathcal{A}_{lm}^{1m}\tilde{\mathcal{B}}_{1m}^{lm}\mathcal{B}_{lm}^{1m}}{\eta_l^{E,1}\tilde{\mathcal{A}}_{1m}^{lm}\mathcal{A}_{lm}^{1m} - \eta_l^{M,1}\tilde{\mathcal{B}}_{1m}^{lm}\mathcal{B}_{lm}^{1m}}, \tag{16a}$$

$$0 = \frac{1}{\eta_l^{M,1}\eta_1^{E,2}} - \tilde{\mathcal{B}}_{1m}^{lm}\mathcal{B}_{lm}^{1m} + \frac{\eta_l^{E,1}\tilde{\mathcal{A}}_{1m}^{lm}\mathcal{A}_{lm}^{1m}\tilde{\mathcal{B}}_{1m}^{lm}\mathcal{B}_{lm}^{1m}}{\eta_l^{E,1}\tilde{\mathcal{A}}_{1m}^{lm}\mathcal{A}_{lm}^{1m} - \eta_l^{M,1}\tilde{\mathcal{B}}_{1m}^{lm}\mathcal{B}_{lm}^{1m}}, \tag{16b}$$

whereby it is evident that in the limiting case of negligible cross-polarization mixing, equations (16) reduce to equations (13). The relative importance of differing approximations and the associated physical effects remains as the topic of future work. In the remainder of this paper equations (11)–(13) will be used, unless otherwise stated, so as to elucidate the dominant physical effects.

The results given here are quite general, however, henceforth only three NP geometries will be considered, specifically isotropic spherical NPs, core–shell NPs and circular cylindrical NPs (or nanorods). Layered NPs, such as the core–shell geometry, and nanorods are particularly attractive as plasmonic NPs, due to the tunability of their optical properties [41–43]. For example, for a core–shell NP, the plasmon resonance frequency can be varied over a wide range of wavelengths by adjusting the ratio of the inner and outer radius, denoted by r_{IV} and r_{III} respectively (see inset of figure 5). Similar resonance tuning can be achieved in nanorods by varying their aspect ratio. Layered NPs are particularly easily treated within the formalism presented here due to their spherical symmetry, whereby it can be shown that $T_{lm,lm}^{\nu\nu} = \kappa_l^{\nu,2}$, where $\kappa_l^{\nu,2}$ describes the scattering from composite NPs (independent of m) including the effects of internal reflections between layers. Expressions for $\kappa_l^{\nu,2}$ for a core–shell NP are given in appendix C, however the reader is referred to the work of Mackowski *et al* [44] for more general configurations. All other elements of the T-matrix are identically zero. For more complicated structures, the T-matrix must be determined numerically, as mentioned earlier.

4. Approximate extinction spectra

Complex roots of equations (12) and (13), denoted k_{lm}^{ν}, give the resonance wavelength and linewidth for a single Mie mode of order (l, m). In practice, however, the azimuthal modes for a single polar index lie in close proximity to each other. Due to their finite widths all such modes must be considered together. When considering scattering from multiple spheres it can be shown that the total extinction spectrum is given by the sum of the extinction spectrum for each sphere individually [45] and in the case under consideration is thus given by

$$P_{\mathrm{ext}} = \frac{\mathrm{i}}{4k^{\mathrm{I}}}\sum_{\nu,lm} l(l+1)k_s^{\mathrm{I}}\mathrm{Re}\left[a_{lm}^{\nu *}b_{lm}^{\nu} + \tilde{a}_{lm}^{\nu *}\tilde{d}_{lm}^{\nu}\right], \tag{17}$$

where, $s = 1, 2$ for $\nu = E, M$ as usual, * denotes complex conjugation and P_{ext} is the total power scattered and absorbed by the WGMR-NP system from the illuminating beam. Neglecting the

illumination field at the NP, as before, allows the second term to be safely ignored. From equation (17) it is evident that to determine the extinguished power, equation (5) must be solved to determine the mode coefficients. Unfortunately this is computationally expensive and it is preferable if such a calculation can be avoided. Accordingly, here an approximate formulation is used, whereby the extinction spectrum in the vicinity of a resonance is represented as a superposition of Lorentzian resonances, with central frequency and linewidths given by the real and imaginary parts of the roots of an appropriate resonance condition. The appropriate amplitude of each Lorentzian is then further found from the illumination coefficients a_{lm}^{ν}.

For example, when considering small spherical NPs the position and width of each resonance is first determined from the roots of equations (13). Given further that equations (13) neglect cross-polarization mixing and coupling between modes of differing polar index l, it is legitimate to assume $b_{lm}^{\nu} = \sigma_{lm}^{\nu} a_{lm}^{\nu}$. For an isolated WGMR it would immediately (and rigorously) follow that $\sigma_{lm}^{\nu} = \eta_l^{\nu,1}$, however for the coupled WGMR-NP system this relation is modified for the $|m| \leqslant 1$ modes. Considering equations (5)–(7) under an electric dipole scattering approximation yields

$$b_{lm}^{E} \approx \eta_l^{E,1} \left[a_{lm}^{E} - \frac{\eta_1^{E,2} \tilde{\mathcal{A}}_{1m}^{lm}}{\mathcal{U}_m} \left(\sum_L \eta_L^{E,1} \mathcal{A}_{Lm}^{1m} a_{Lm}^{E} + \frac{k_2^{\mathrm{I}}}{k^{\mathrm{I}}} \eta_L^{M,1} \mathcal{B}_{Lm}^{1m} a_{Lm}^{M} \right) \right] \tag{18}$$

for $|m| \leqslant 1$ and an analogous expression for b_{lm}^{M}, where

$$\mathcal{U}_m = \eta_1^{E,2} \sum_L \left(\eta_L^{E,1} \tilde{\mathcal{A}}_{1m}^{Lm} \mathcal{A}_{Lm}^{1m} + \eta_L^{M,1} \tilde{\mathcal{B}}_{1m}^{Lm} \mathcal{B}_{Lm}^{1m} \right) - 1. \tag{19}$$

Neglecting cross-polarization mixing and coupling between modes of differing polar index therefore gives

$$\sigma_{lm}^{E} \approx \eta_l^{E,1} \left[1 - \eta_l^{E,1} \eta_1^{E,2} \frac{\tilde{\mathcal{A}}_{1m}^{lm} \mathcal{A}_{lm}^{1m}}{\mathcal{U}_m} \right], \tag{20a}$$

$$\sigma_{lm}^{M} \approx \eta_l^{M,1} \left[1 - \eta_l^{M,1} \eta_1^{E,2} \frac{\tilde{\mathcal{B}}_{1m}^{lm} \mathcal{B}_{lm}^{1m}}{\mathcal{U}_m} \right]. \tag{20b}$$

Similar expressions were derived in the work of Deych and Rubin [29, 40] for dielectric spherical Rayleigh scatterers. By virtue of their dependence on the scaling parameters $\eta_l^{\nu,j}$ (or $\kappa_l^{\nu,2}$ when considering core–shell NPs), σ_{lm}^{ν} exhibit a wavelength dependence. This can be approximated by the complex Lorentzian function

$$\sigma_{lm}^{\nu}(k) \approx \sigma_{lm}^{\nu}(k_0) \frac{\mathrm{i}\Gamma_0/2}{(k - k_0) + \mathrm{i}\Gamma_0/2}, \tag{21}$$

where $\sigma_{lm}^{\nu}(k_0)$ is real, $k_0 = \mathrm{Re}\left[k_{lm}^{\nu}\right]$ and $\Gamma_0 = -2\,\mathrm{Im}\left[k_{lm}^{\nu}\right]$. Hence, finally

$$P_{\mathrm{ext}} \approx \frac{i}{4k^{\mathrm{I}}} \sum_{\nu,lm} l(l+1) k_s^{\mathrm{I}} \frac{\Gamma_0^2\, \sigma_{lm}^{\nu}(k_0)}{4(k - k_0)^2 + \Gamma_0^2} |a_{lm}^{\nu}|^2 \tag{22}$$

which can easily be measured in a practical experiment, for example, by monitoring the optical throughput of the coupling fibre.

If resonance conditions are formed by diagonalizing $\mathbb{A}\mathbb{A}$ (see section 3), as is appropriate for more general NP geometries, the simple scaling relation $b_{lm}^{\nu} = \sigma_{lm}^{\nu} a_{lm}^{\nu}$ no longer holds and

equations (18), (20) and (22) require modification. In particular, neglecting $\mathbb{A}_3$ and $\mathbb{A}_4$ terms, it can be shown (see appendix D for a brief derivation) that

$$\mathbf{b}^{\nu} \approx \mathbb{N}^{\nu,1}\left(\mathbb{I} + \left[\mathbb{I} - \mathbb{A}_s\mathbb{N}^{\nu,1}\right]^{-1}\mathbb{A}_s\mathbb{N}^{\nu,1}\right)\mathbf{a}^{\nu} = \mathbb{S}^{\nu}\mathbf{a}^{\nu}. \tag{23}$$

Equation (23) reduces to equation (18) for spherical NPs. In practice the full matrix relation defined by equation (23) need not be used, since for small NPs only the $|m| \leqslant 1$ modes are perturbed such that only a 3×3 subblock of $\mathbb{S}^{\nu}$ differs from the isolated WGMR case (also neglecting coupling between modes of different l index). To restore an equation of the form of equation (22) it is further necessary to express $\mathbf{a}^{\nu}$ and $\mathbf{b}^{\nu}$ in the eigenbasis of $\mathbb{A}\mathbb{A}$ as given by $\bar{\mathbf{a}}^{\nu} = \mathbb{V}^{-1}\mathbf{a}^{\nu}$ and $\bar{\mathbf{b}}^{\nu} = \mathbb{V}^{-1}\mathbf{b}^{\nu}$, where $\mathbb{V}$ denotes the matrix formed from the eigenvectors of $\mathbb{N}^{\nu,1}\mathbb{A}_s$. Again it is noted that for small NPs only a 3×3 subblock of $\mathbb{V}$ will differ from the identity matrix. Equation (22) can then be used to calculate the approximate extinction coefficient with the replacement $a^{\nu}_{lm} \to \bar{a}^{\nu}_{lm}$ for $|m| \leqslant 1$ and where σ^{ν}_{lm} are given by the diagonal elements of $\mathbb{V}^{\dagger}\mathbb{S}^{\nu}\mathbb{V}$.

To illustrate the possible consequences of equation (22), it is informative to consider a fundamental WGM excited in an isolated WGMR, that is to say one in which the majority of the mode intensity lies in a single plane. Commonly, a fundamental mode of polar index l is described by a single azimuthal mode of index $|m| = l$, i.e. in a coordinate system in which the z-axis lies perpendicular to the plane of the mode (see e.g. the work of Teraoka and Arnold [17] and many others). It is important to re-emphasize, however, that in this paper a different convention is adopted as discussed above, whereby the z-axis is chosen so as to join the centres of the WGMR and the perturbing NP. The resonance in the extinction spectrum for an isolated WGM is thus formed by the superposition of $2l + 1$ degenerate modes (as shown schematically in the top panel of figure 2), with strengths that can be determined from the Wigner-D functions [33]. The inset of figure 2, for example, shows the mode strengths for a $l = 40$ fundamental WGM, assuming the polar axis is taken to lie in the same plane as the WGM.

If a perturbing NP is brought into close proximity to the WGMR the increased coupling causes the low azimuthal modes to shift, whilst the higher order modes remain unshifted, as discussed in section 3. If the coupling strength is not too strong, the shift of the low order azimuthal modes is smaller than the linewidth of the original WGM resonance, such that the total spectrum exhibits a small shift in peak position (middle panel of figure 2, assuming a TM fundamental WGM, such that the $|m| = 1$ and $m = 0$ modes are all shifted, albeit by differing amounts). Whilst inherent line broadening (from increased scattering/coupling losses) of each individual azimuthal mode has been neglected in the schematic of figure 2, broadening of the aggregate resonance nevertheless results due to the shift of low order modes. Finally, if the coupling strength is strong enough (e.g. for larger NP polarizability or close proximity), the shifts of the low order azimuthal modes, can be large enough so as to produce multiple peaks in the extinction spectrum, i.e. mode splitting (bottom panel). For the TM mode, this can give rise to a triplet as seen in the bottom panel of figure 2, whilst for the TE case only a doublet is produced, since the $m = 0$ mode does not shift [33]. To date only doublets have been experimentally observed e.g. [28], however experimental methods by which to verify the triplet nature of splitting in the TM case are proposed in [29, 40]. It is, however, plausible that such a triplet will ultimately, be unobservable, either due to NP induced losses introduced into the $m = 0$ mode which may appreciably degrade the quality of the resonance, or because

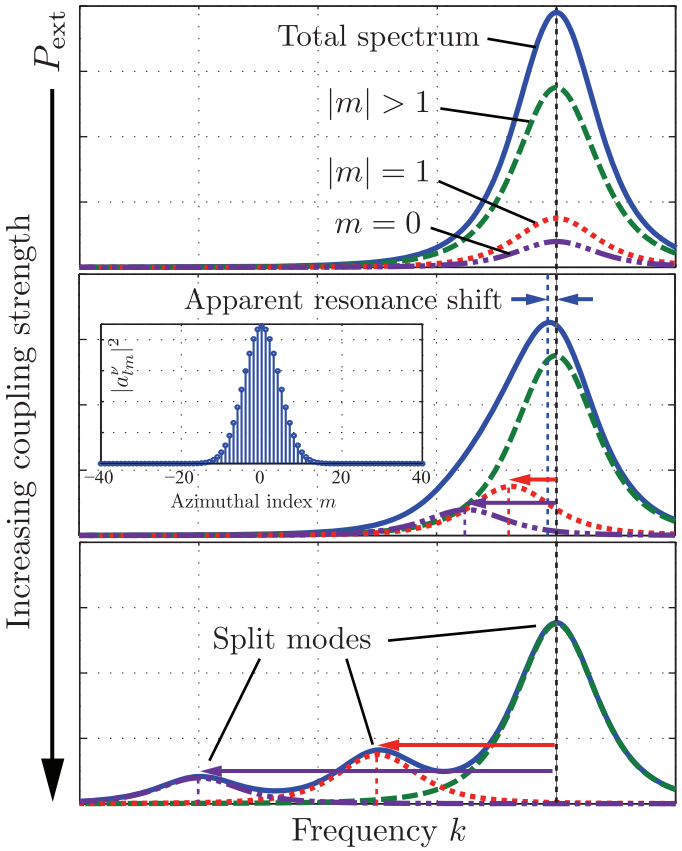

Figure 2. Schematic representation of the origin of apparent WGM shifts versus mode splitting, based on the shift of low azimuthal modes only. (inset) Mode strengths of degenerate azimuthal modes in a fundamental $l = 40$ WGM.

illumination optics also alter the resonant mode structure [46], such that the $m = 0$ mode degeneracy is lifted. This, however, remains an open experimental question.

5. Results

5.1. Dielectric and solid metallic spherical nanoparticles—model validation and mode splitting

Given the theoretical derivations presented above, a number of studies will be discussed here, through which the coupling between WGMRs and plasmonic NPs is investigated. By way of initial validation of the theory, however, a preliminary study of perturbation of a WGMR by a small spherical dielectric particle is considered. This scenario has been well studied in the literature and resonance shifts are usually determined by applying a first order perturbation approximation to the vectorial wave equations [16, 17]. Under this approximation the resonance shift can be shown to be given by

$$\frac{\delta k_0}{k_0} \approx -\frac{(\epsilon_{\mathrm{III}} - \epsilon_{\mathrm{I}})}{2} \frac{\int_{V_{\mathrm{III}}} \mathbf{E}^*(\mathbf{r}) \cdot \mathbf{E}'(\mathbf{r}) \mathrm{d}\mathbf{r}}{\int_V \epsilon(\mathbf{r}) \, |\mathbf{E}(\mathbf{r})|^2 \, \mathrm{d}\mathbf{r}}, \tag{24}$$

where $\mathbf{E}^{(\prime)}(\mathbf{r})$ is the electric field before (after) introduction of the NP, V_{III} denotes the volume of the NP and V denotes all space. Here $\epsilon(\mathbf{r})$ is the permittivity distribution before introduction of the NP, such that $\epsilon(\mathbf{r}) = \epsilon_{\mathrm{II}}$ for $\mathbf{r} \in V_{\mathrm{II}}$ and ϵ_{I} otherwise. Due to the computational burden in determining the perturbed field $\mathbf{E}'(\mathbf{r})$, recourse is customarily made to a quasi-static approximation to determine the perturbed field, $\mathbf{E}'(\mathbf{r})$ yielding [15]

$$\frac{\delta k_0}{k_0} \approx -\frac{\mathrm{Re}[\alpha]}{2} \frac{|\mathbf{E}(\mathbf{r}_{\mathrm{NP}})|^2}{\int_V \epsilon(\mathbf{r})\,|\mathbf{E}(\mathbf{r})|^2\,\mathrm{d}\mathbf{r}}, \tag{25}$$

where α is the excess polarizability of the perturbing particle. Note that the domain of integration for the integral in the denominator of equation (25) is also commonly taken as V_{II}, i.e. the spatial extent of the WGMR, since this contains the majority of energy of the WGM. This approximation is not made in this paper.

Predictions of the shift in resonance wavelength, based on equation (25), of the $l = 40$ fundamental WGM in a polycarbonate WGMR (with refractive index $n_{\mathrm{II}} = 1.59$ and radius $r_{\mathrm{II}} = 4\,\mu$m) in air ($n_I = 1$) from the introduction of a dielectric NP (of radius $r_{\mathrm{III}} = 32\,$nm) at a fixed centre to centre distance of $4.1\,\mu$m are shown in figure 3 as a function of the refractive index n_{III} of the perturbing NP. Consideration is here limited to the second order radial resonance, with a Q factor of approximately 10^5, since the first order radial mode, with a Q factor of $\sim 10^7$, is harder to observe experimentally. Furthermore the second order mode lies in a wavelength range (for the WGMR size chosen here) that has been used in realistic biosensing applications [32]. Practically Q factors will also be reduced further from the values quoted here, due to material absorption, surface roughness and other defects invariably present in WGMRs. For reference purposes, the radial distributions of the first three radial modes are shown in the inset of figure 3, in conjunction with the effective trapping potential imposed by the WGMR boundary [47]. Higher order radial modes exhibit greater tunnelling through the potential barrier, such that radiation losses are higher, resulting in the reduced Q factor.

Calculation of equation (25) assumed the field present before introduction of the NP (i.e. $\mathbf{E}(\mathbf{r})$) to be a pure $l = 40$ fundamental WGM. For simplicity, in all calculations, it is also assumed that the NP (and hence the polar axis) lies in the plane of the fundamental mode, although this does not reflect any such restriction to the formalism. Accordingly, the resonance position for all azimuthal modes can be determined from equations (13) and the shift in the maximum of the extinction spectrum, calculated via equation (22), determined. Root finding algorithms, as required for the solution of equations (13), could be said to bring an undesirable level of complication to determining resonance shifts. As such, instead of numerical root finding, approximate roots to equations (13) were derived and found to agree well with exact roots. Specifically, by adopting a complex Lorentzian approximation to the scaling parameter $\eta_l^{\nu,1}$ (analogously to equation (21)), the shift in resonance wavenumber can be shown to be approximately given by

$$\delta k_0 = \frac{\Gamma_0}{2} \eta_l^{E,1} \mathrm{Re}\left[i\,\eta_1^{E,2} \tilde{\mathcal{A}}_{1m}^{lm} \mathcal{A}_{lm}^{1m}\right] \text{ for TM modes,} \tag{26a}$$

$$\delta k_0 = \frac{\Gamma_0}{2} \eta_l^{M,1} \mathrm{Re}\left[i\,\eta_1^{E,2} \tilde{\mathcal{B}}_{1m}^{lm} \mathcal{B}_{lm}^{1m}\right] \text{ for TE modes,} \tag{26b}$$

where all quantities are evaluated at the original resonance frequency k_0. To determine the resonance frequency of the isolated WGM numerical root finding methods were employed, where asymptotic formulae found in the literature [48, 49] where used as the initial starting seed.

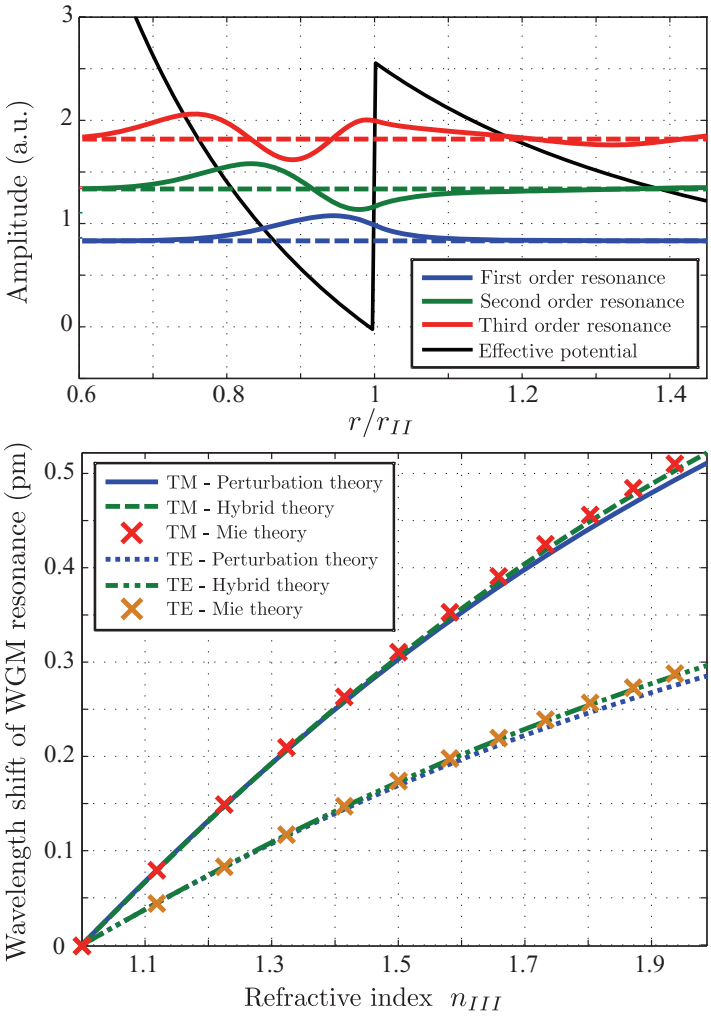

Figure 3. (top) Radial mode amplitude distributions for the first three radial resonances of the $l = 40$ WGM, in relation to the effective trapping potential. Vertical placement of distributions is for visual purposes only. (bottom) Theoretical resonances shifts for the $l = 40$ TE and TM WGMs supported in a polycarbonate spherical resonator when perturbed by a dielectric NP of varying refractive index.

Likewise, the broadening of each resonance, $\delta\Gamma_0$, can be shown to be given by similar equations to equation (26), albeit the imaginary part is taken instead of the real part. It should also be noted that in the quasi-static limit $\eta_1^{E,2}$ can be shown to be proportional to the polarizability of the NP, in agreement with equation (25). Equations (26) (and the broadening counterparts) are only valid when the NP is far from any resonances. The resonance shifts calculated using this method (which shall be referred to as the hybrid resonance theory) are also shown in figure 3 for comparison. As a final remark on the calculation of resonance shifts, it is important to mention that illumination coefficients a_{lm}^{ν} must be chosen and normalized correctly, so as to compare equivalent fields in both calculations (see e.g. Deych *et al* [33]). Significant differences between the resonance shifts calculated by these two methods result if different illuminations are used.

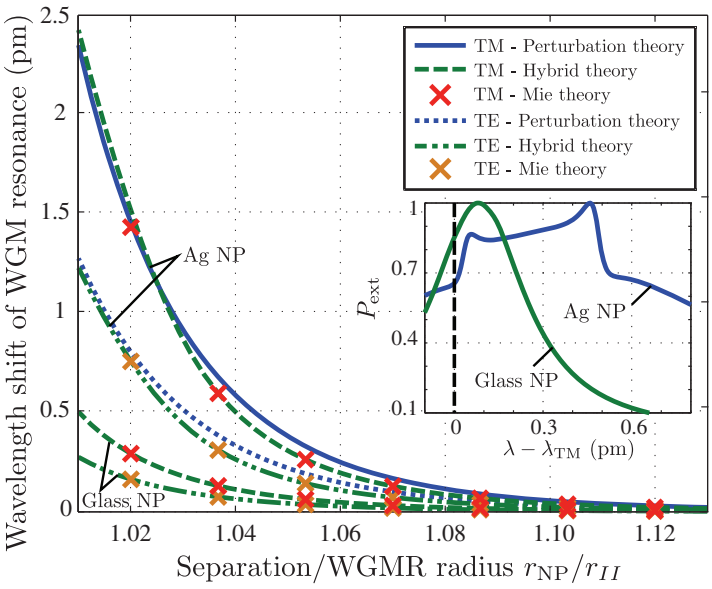

Figure 4. Theoretical resonances shifts for the $l = 40$ TE and TM WGMs supported in a polycarbonate spherical resonator when perturbed by a glass and metallic NP. (inset) Normalized extinction spectrum of a first order WGM when perturbed by a glass and metallic NP, exhibiting mode splitting in the latter case.

The resonance shift, as determined from solution of the full Mie scattering problem is also shown in figure 3 by way of further, and rigorous, validation. Close agreement between all three calculation methods is evident, for both TE and TM resonances, as expected.

Plasmonic resonances are only exhibited in metallic structures, and thus attention is now turned to this scenario. Silver (or silver-based) NPs are, however, exclusively considered in this work, since they exhibit a stronger and higher quality plasmon resonance in visible wavelengths than copper or gold NPs and thus can induce larger resonance shifts. In particular, this effect is a consequence of the small spectral overlap between the plasmon resonance and interband transitions in silver, which would otherwise result in an additional damping mechanism, thus weakening and broadening the resonance. In this vein, figure 4 shows the resonance shifts determined from equations (13) and exact Mie scattering calculations, for a solid silver NP, as a function of WGMR-NP separation, r_{NP}. Since the dielectric function of small metal particles becomes size dependent when the NP size is small in relation to the mean-free path of electrons in bulk metal the dielectric function

$$\epsilon_{III}(\omega) = \epsilon_\infty - \frac{\omega_p^2}{\omega^2 + \gamma^2} + i\frac{\omega_p^2 \gamma}{\omega(\omega^2 + \gamma^2)} \tag{27}$$

was used [50], where ϵ_∞ is the optical dielectric constant at infinite frequency and ω_p is the plasma frequency. Furthermore $\gamma = \gamma_0 + \Delta\gamma$, where γ_0 is a bulk damping term and $\Delta\gamma = v_F/\bar{l}$ is a size dependent damping term accounting for electron surface interactions, as determined by the Fermi velocity v_f and the electron mean free path $\bar{l}$. For this study the values $\epsilon_\infty = 3.7$, $\omega_p = 8.9\,\text{eV}$, $\gamma_0 = 0.021\,\text{eV}$ and $v_f = 1.4 \times 10^6\,\text{ms}^{-1}$ were assumed and the electron mean free path was determined as in [51]. It should be noted that particle dimensions were chosen such that size dependent effects did not degrade the quality of the surface plasmon resonance greatly.

Good agreement between all three calculation methods is found once more as expected, with the silver NP exhibiting more than a four-fold enhancement of the resonance shift of the WGM, with respect to the glass NP.

Finally, and in reference to the inset of figure 4, attention is briefly given to the first radial order TM mode in a polycarbonate WGMR, with a resonance wavelength of 859.112 nm and a Q factor of $\sim 1.5 \times 10^7$. In particular the inset of figure 4 shows the normalized spectrum around the WGM resonance when both a glass and silver NP are placed close to the WGMR surface. In the former case, line broadening and a shift is evident, in a similar manner to that discussed thus far. For the silver NP, however, mode splitting is evident, therefore highlighting the greater ease with which mode splitting can be observed when using plasmonic NPs. It is important to note, that the extinction spectra presented in the inset of figure 4 do not correspond to those used to calculate the shifts depicted in the main panel. Indeed, when mode splitting occurs it is no longer meaningful to define a WGM resonance shift.

5.2. Core–shell nanoparticles—mode hybridization and level repulsion

Despite the good agreement seen in the previous section, it should be recognized that the localized plasmon resonance of the silver NP lies at a wavelength of 357.477 nm, whilst the TM and TE WGM resonances considered here occur at wavelengths of 772.459 and 782.922 nm respectively. Consequently, the resonance properties of the NP are negligible and the enhancement of the resonance shift follows by virtue of the off-resonance permittivity. In this case, when no mode splitting was evident, perturbation theory was found to give good results in relation to the more exact theory presented here. Tunability of the plasmon resonance frequency in core–shell NPs, however, enables further enhancement of the WGM shift, by bringing the plasmon resonance frequency close to the WGM resonance frequency. In so doing, coupling between the WGMR and NP is increased due to the increased spectral overlap of the resonances. Coupled resonators, however, imply that each resonator system can no longer be considered in isolation, but instead hybrid WGMR-NP resonant modes must be found. Equations (13) give precisely the resonance conditions for such hybrid modes, with the replacement $\eta_1^{\nu,2} \to \kappa_1^{\nu,2}$.

To first demonstrate the increased coupling strength, and hence larger resonance shifts, the shift in resonance frequency of the $l = 40$ WGM resonance was calculated, as a core–shell NP ($r_{\mathrm{III}} = 55$ nm) is brought closer to the WGMR surface and is shown in figure 5. A fused silica core ($n_{\mathrm{IV}} = 1.48$) and a silver shell were assumed. The dipole plasmon resonance of the NP was tuned to lie 10 nm below the WGM resonance, such that the ratio of the outer to inner radius $f = r_{\mathrm{III}}/r_{\mathrm{IV}}$ was $\sim$0.9139 and 0.9166 for the TM and TE modes respectively. With reference to figure 5, an enhancement of the resonance shift of approximately $\times 60$ is apparent, however discrepances between the first order perturbation results (equation (25)) and those found from use of equations (13) are now evident. Disagreement between the two theories results from a failure in the quasi-static approximation to account for retardation effects and spatial variations of the induced field across the extent of the NP, which can be strong (particularly within the shell near resonance). Furthermore, the quasi-static approximation does not account for back-action of the NP upon itself, i.e. multiple scattering effects. Whilst figure 5 shows a $>30\%$ discrepancy between the perturbation theory and hybrid resonance calculations, it should be noted that the magnitude of the difference depends on a number of factors, such as NP dimensions, resonance detuning and WGM order. Study of these effects is beyond the scope of this paper.

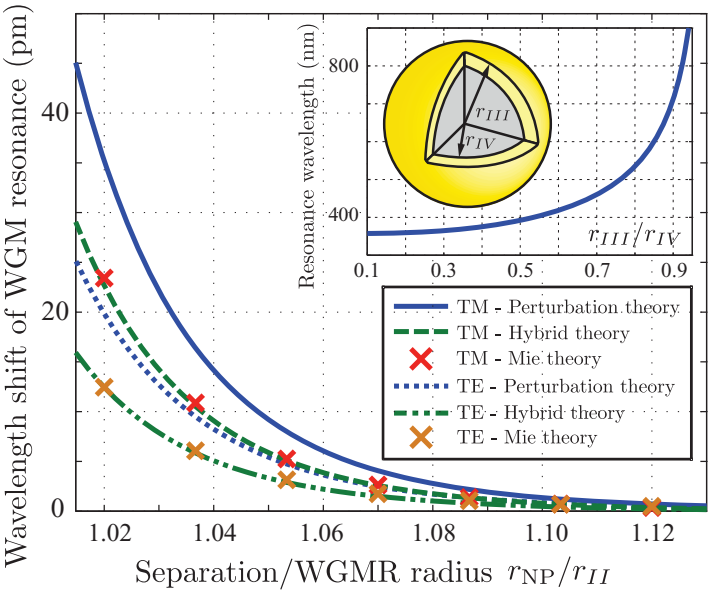

Figure 5. As figure 4, but for perturbation of the WGMR by a core–shell NP, with dipole plasmon resonance tuned to lie 10 nm below the WGM resonance. (inset) Geometry of a core–shell NP and the dipole plasmon resonance wavelength as a function of the ratio of the core and shell radii.

Approximate expressions for the roots of equations (13) can again be derived, which highlight the hybridized nature of the resonant modes. Derivation proceeds as in section 5.1, except, now both $\eta_l^{\nu,1}$ and $\kappa_l^{\nu,2}$ are approximated by complex Lorentzians, yielding a complex quadratic equation in the new hybrid resonance frequency. Denoting the (complex) resonant frequencies of the isolated WGMR and NP as $k_{lm}^{\nu,j} = k_j = k_{0,j} - \mathrm{i}\Gamma_{0,j}/2$ for $j = 1$ and 2 respectively, standard methods can be used to complete the square, yielding

$$\delta k_j = \frac{1}{2}\left[\left(k_1 + k_2 - 2k_j\right) \pm \sqrt{(k_1 - k_2)^2 - K}\right], \tag{28}$$

where the $\pm$ sign is adopted for $j = 1, 2$ respectively, $K = \Gamma_{0,1}\Gamma_{0,2}\eta_l^{E,1}(k_{0,1})\kappa_1^{E,2}(k_{0,2})\tilde{\mathcal{A}}_{1m}^{lm}\mathcal{A}_{lm}^{1m}$ for quasi-TM modes and $\Gamma_{0,1}\Gamma_{0,2}\eta_l^{M,1}(k_{0,1})\kappa_1^{E,2}(k_{0,2})\tilde{\mathcal{B}}_{1m}^{lm}\mathcal{B}_{lm}^{1m}$ for quasi-TE resonances. Equation (28), in reality, is a transcendental equation for the shifted resonant frequency (as opposed to giving the resonance shift directly) of the three lowest order azimuthal modes ($|m| \leqslant 1$), owing to the strong wavelength dependence of the translation coefficients ($\mathcal{A}_{lm}^{1m}$, etc). Nevertheless, given that the remaining higher order modes, which also contribute to the extinction spectrum, remain unshifted, and that for practical WGMRs l is large, the wavelength dependence of the translation coefficients has negligible effect, such that it is sufficient to evaluate them at $k_{0,j}$ (further justification can be found in [52]). Under the circumstances considered in this work $|K/(k_1 - k_2)^2| \ll 1$ such that equation (28) simplifies to

$$\delta k_j = \mp\frac{1}{4}\frac{K}{k_1 - k_2}. \tag{29}$$

By taking the real and imaginary parts of equations (28) or (29), the shift in resonant frequency and broadening of the hybrid resonances quickly follows.

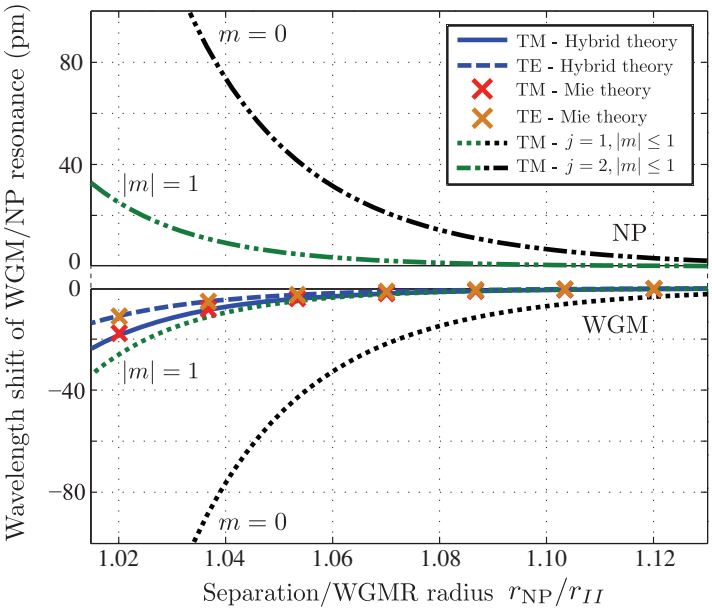

Figure 6. Theoretical resonances shifts of the $j = 1$ and 2 TM and TE hybrid photonic–plasmonic modes of a WGMR-NP system as the core–shell NP, with dipole plasmon resonance tuned to lie 10 nm above the isolated WGM resonance, approaches the WGMR.

Inspection of equation (29) reveals two features of interest to biosensing applications (and beyond). Firstly, and considering only the $j = 1$ mode, it is evident that if $k_{0,1} > k_{0,2}$, the presence of the NP appears to red shift the WGM, as it approaches the WGMR. Red shifts, of this nature are, for example, seen in figures 4 and 5. However, tunability of the plasmon resonance affords the possibility that $k_{0,1} < k_{0,2}$, such that blue shifts can be recorded. To date, observation of blue shifts has only been possible in sensing applications if the refractive index of the perturbing NP is less than the immersion medium (n_I) [40]; a criteria rarely fulfilled in practice. Secondly, equation (29) shows that the $j = 2$ mode is shifted in the opposite sense to the $j = 1$ mode. Since the $j = 2$ mode corresponds to the surface plasmon resonance in the isolated NP, equation (29) describes level repulsion between the NP and WGMR as the coupling strength, K, is increased. Level repulsion of this nature is common to many hybridization phenomena [53] and is illustrated in figure 6 for a similar situation to the results of figure 5, albeit the NP resonance is now tuned to lie 10 nm above the WGM resonance. Specifically, blue curves in figure 5 depict the aggregate shift of the initial WGM, which is towards shorter wavelengths (i.e. blue shifts), whilst the green and black curves show the shift of a single azimuthal mode ($|m| \leqslant 1$), for both $j = 1$ and 2. Notably, the shifts for the individual $|m| \leqslant 1$ azimuthal modes are larger than typical experimental WGM shifts, however, it is again emphasized that the total aggregate shift is formed by the superposition of a large number of unshifted modes and a small number of shifted modes as discussed in section 4. Furthermore the shift of the $|m| \leqslant 1$ mode is larger than the initial line-width of the WGM such that mode splitting might be expected. Crucially, however, NP induced losses broaden the WGM to such an extent that this is not the case. Mode broadening of this form, potentially, allows the domain of perturbation based calculations to be extended, albeit care must still be taken if the quasi-static formulation is used.

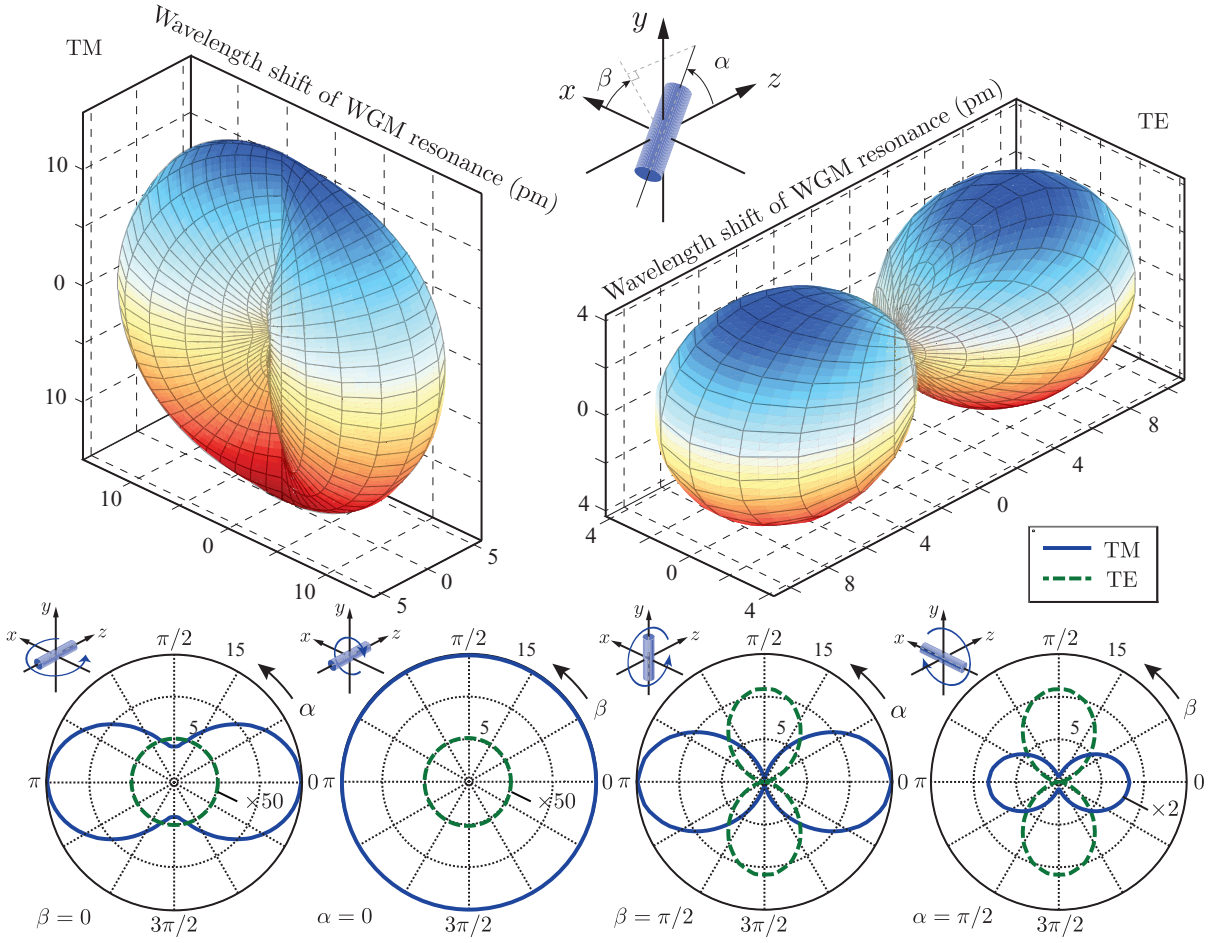

Figure 7. (top middle) Schematic showing definition of Euler angles α and β which determine the orientation of the long axis of a cylindrical nanorod. (top left/right) Spherical polar plot (with polar angles α and β) in which the radius is given by the magnitude of the resonance shift of the TM/TE WGM (in pm). (bottom row) Polar plots showing cross-sections of the full spherical polar plots for rotation of the nanorod in the x–z plane around its short axis, x–y plane around its long axis, y–z plane around its short axis and x–y plane around its short axis (left to right). All shifts of the WGM resonance are towards the red end of the spectrum.

As a final point, it is noted that given the plasmon resonance is excited through leakage from the WGMR, it is only excited weakly and cannot be easily seen in the extinction spectrum.

5.3. Metallic nanorods—orientational dependence

Similarly to core–shell NPs, nanorods afford the opportunity for tuning of the localized plasmon resonance frequency by variation of the aspect ratio and physical size [42]. Additionally, nanorods also exhibit much stronger near field enhancements than core–shell NPs due to the sharper geometrical features, hence motivating their use in sensing applications. Due to the lack

of spherical symmetry shifts of WGM resonances from nanorods, however, intrinsically show a dependence on the orientation of the nanorod relative to the WGMR surface. As previously mentioned in sections 3 and 4, rotational symmetry around the polar axis implies that the NP possesses a T-matrix which is diagonal with respect to m. This is indeed the case for a nanorod aligned parallel to the z-axis, however, if the nanorod is rotated with respect to the z-axis, the T-matrix can have strong off-diagonal elements, necessitating diagonalization of the perturbing matrix (i.e. $\mathbb{A}\mathbb{\Lambda}$). Adopting this approach, and assuming the same WGMR parameters as above, the resonance shifts for the $l = 40$ TM and TE WGM were calculated for perturbation by a cylindrical silver nanorod (with radius 25 nm and a length of 125 nm), placed at a distance of 140 nm from the surface of the WGMR for different nanorod orientations. The nanorod dimensions were selected so as to place the longitudinal plasmon resonance of the nanorod at approximately 758 nm. For simplicity, size dependent effects in the dielectric function were disregarded for this calculation. An arbitrary rotation of a three-dimensional object can be described by the associated Euler angles (α, β, γ), however, given the axial symmetry of nanorods γ can be set to zero without loss of generality. Accordingly the long axis of the nanorod is completely specified by (α, β) as depicted in figure 7 (top-middle). Determination of the T-matrix of the rotated NP follows by applying the rotation transformation rule to the T-matrix of the unrotated (i.e. parallel to z) nanorod [35]. Numerical results for the resonance shifts are shown in figure 7, wherein the top left and right panels, present spherical polar surface plots, in which the radius at each orientation represents the magnitude of the resonance shift. Due to the relative spectral position of the WGM and plasmon resonances, the WGM resonance is red-shifted regardless of nanorod orientation. Numerous cross-sections of the surface plots are also shown in figure 7 (bottom row of polar plots), in which, the radius again represents the magnitude of the resonance shift. In turn, the polar plots represent rotation of the nanorod in the x–z plane around its short axis, x–y plane around its long axis, y–z plane around its short axis and, finally, in the x–y plane around its short axis. Some results have been scaled for clarity, as noted in figure 7. Given that the TM WGM has non-zero electric field components in the x and z directions, whilst the TE WGM only has a non-zero field component in the y direction, it is seen that greater resonance shifts result when the long axis of the nanorod is aligned with a non-zero component of the unperturbed WGM mode. In this case coupling to the longitudinal plasmon resonance is high, such that resonance shifts are larger, in accordance with physical intuition. Interestingly, it should be noted that if the long axis of the nanorod is orthogonal to a non-zero field component, non-zero shifts can still result due to the off-resonance permittivity of the nanorod and weak excitation of the transverse plasmon resonance. Finally, it is again emphasized that good agreement was found between the results presented in figure 7 and those found by performing full Mie scattering calculations.

6. Discussion

Theoretical derivations presented in this paper, have sought to describe the effect of metallic NPs upon the resonant modes of larger dielectric spheres, particularly with a view towards WGM biosensing. Whilst first order perturbation theory gives approximate expressions for a perturbed WGMR (which have seen extensive use and verification in the literature), problems can result when considering resonant NPs. For example, whilst equation (25) can be computed rapidly, near NP resonances it gives inaccurate predictions due to the implicit quasi-static approximation. On the other hand, equation (24) can produce more accurate results, however

this comes at the expense of increased computational burden, since the perturbed field, $\mathbf{E}'(\mathbf{r})$, must be determined numerically and subsequently spatially integrated. In an attempt to mitigate these problems, resonance conditions of the hybrid WGMR-NP system were therefore established based upon rigorous scattering (Lorenz–Mie) theory, from which shifts in resonance frequency can be easily determined. Specifically the hybrid resonances are determined by finding (complex) roots of the system matrix, from which the extinction spectrum can be determined in an approximate manner. In general, analytical solution of the system equations is intractable, however approximate closed form analytic formula were established (equations (11)–(13)) by approximating the related eigenvalue equation.

Small NPs, which can be considered as electric dipole scatterers, allow the resonance conditions to be expressed in a particularly simple form (equations (13)), further facilitating analytic analysis. In light of the desire to avoid unnecessary calculations, for example, approximate formulae were derived for the resonance shift and resonance broadening, from interaction of a NP with a WGMR. It should be noted that the latter represents an advantage over the first order perturbation calculations. Despite the approximations made, the hybrid resonance conditions were found to agree well with full Mie scattering calculations.

Given the greater generality of Lorenz–Mie scattering theory, a number of further advantages over first order perturbation theory can be identified. Especially prominent is the richer array of physical phenomena which can be predicted and described, a number of which have been presented in this work. For example, mode splitting was demonstrated to occur under less stringent conditions for metallic NPs, than for dielectric NPs. The question, however, still remains, as to the precise criteria for observation of mode splitting, since line broadening (also describable within the Lorenz–Mie formalism) is also more significant for metallic NPs. Accordingly a balance between reactive (inductive) and resistive coupling must be struck to observe splitting. Mode hybridization, and level repulsion, were also seen to naturally emerge from the derived hybrid resonance conditions. This was, for example, shown to occur between TM and TE WGMs, when cross-polarization mixing was considered (see equations (16)) and between the WGM and plasmon resonances that can exist in metallic NPs (e.g. equations (28) and (29)). Given the occurrence of level repulsion in a hybrid WGMR-NP system, by careful tuning of the plasmon resonance of the isolated NP (e.g. a core–shell NP), blue shifts of the WGM resonance can be obtained. Within the context of biosensing, this hence presents an immediate means by which detection multiplexing can be achieved. Use of, for example, two different NPs, each functionalized for detection of different biomolecules, and designed so as to induce red and blue WGM resonance shifts respectively, allows discrimination of two different biomolecules.

Finally, Lorenz–Mie theory provides a natural framework, which can be extended to exploit Waterman's extended boundary method and thus to describe non-spherical NPs, such as nanorods and nanocubes. In this vein, a study of the dependence of resonance shifts on nanorod orientation was presented. Whilst for more common NP geometries numerous efficient codes already exist, it should be noted that ill conditioning and/or poor convergence may hamper determination of the T-matrix for more exotic geometries. Moreover, algorithms for calculation of the T-matrix, must allow for complex frequencies, since solutions to the resonance condition are found on the complex plane. Fortunately, this, in principle, does not require any major additional coding efforts to be made. In the context of biosensing, knowledge of the dependence of resonance shifts on orientation of asymmetric nanorods affords the possibility of orientational binding studies. For example, by monitoring resonance shifts in both the TE and

TM polarization channels, and with *a priori* knowledge regarding the nanorod properties, the orientation of a perturbing nanorod can be inferred. This, however, remains as future work.

Appendix A. Definition of the Mie modes

The electric fields of the electric and magnetic multipole fields, or Mie modes, can be expressed in terms of spherical field components (E_r, E_θ, E_ϕ) as [54]

$$\mathbf{E}_{lm}^{E(j)}(\mathbf{r}) = \begin{bmatrix} l(l+1)\frac{h_l^{(j)}(kr)}{r} Y_l^m(\theta,\phi) \\ \frac{1}{r}\frac{\mathrm{d}}{\mathrm{d}r}(r h_l^{(j)}(kr))\frac{\partial}{\partial\theta} Y_l^m(\theta,\phi) \\ \frac{\mathrm{i}m}{r\sin\theta}\frac{\mathrm{d}}{\mathrm{d}r}(r h_l^{(j)}(kr)) Y_l^m(\theta,\phi) \end{bmatrix}, \tag{A.1a}$$

$$\mathbf{E}_{lm}^{M(j)}(\mathbf{r}) = \begin{bmatrix} 0 \\ \frac{\mathrm{i}k_2 m}{\sin\theta} h_l^{(j)}(kr) Y_l^m(\theta,\phi) \\ -k_2 h_l^{(j)}(kr)\frac{\partial}{\partial\theta} Y_l^m(\theta,\phi) \end{bmatrix}, \tag{A.1b}$$

where $h_l^{(j)}(kr)$ can be either a spherical Hankel ($j = 1, 2$) or a spherical Bessel ($j = 3$) function. $Y_l^m(\theta,\phi)$ are the spherical harmonics of order $l = 1, 2, 3, \ldots, m = -l, -l+1, \ldots, l$ defined by

$$Y_l^m(\theta,\phi) = \left[\frac{(2l+1)(l-m)!}{4\pi(l+m)!}\right]^{1/2} P_l^m(\cos\theta)\exp(\mathrm{i}m\phi), \tag{A.2}$$

where $P_l^m(\cdot)$ are the associated Legendre polynomials. The multipole modes depend on the material properties via the constants $k_1 = \mathrm{i}\omega\epsilon - \sigma/\omega$, $k_2 = \mathrm{i}\omega\mu$, where $k^2 = -k_1 k_2$, ϵ is the permittivity of the medium, μ is the permeability and σ is the conductivity [55]. The corresponding magnetic fields are given by $\mathbf{H}_{lm}^{M(j)}(\mathbf{r}) = \mathbf{E}_{lm}^{E(j)}(\mathbf{r})$ and $\mathbf{H}_{lm}^{E(j)}(\mathbf{r}) = -\frac{k_1}{k_2}\mathbf{E}_{lm}^{M(j)}(\mathbf{r})$.

Appendix B. Mie expansions in shifted coordinate systems

Consider two coordinate systems in which a point is described by the position vectors $\mathbf{r}$ and $\mathbf{r}'$ respectively, where $\mathbf{r}' = \mathbf{r} - \mathbf{r}_{\mathrm{NP}}$ (see figure 1). Any field can be represented using Mie expansions in both coordinate systems. Consider representing a field $\mathbf{E}(\mathbf{r})$ in terms of Mie modes centred on $\mathbf{r} = 0$ and $\mathbf{r}' = 0$, such that

$$\mathbf{E}(\mathbf{r}) = \sum_{l,m} a_{lm}^E \mathbf{E}_{lm}^{E(j)}(\mathbf{r}) + a_{lm}^M \mathbf{E}_{lm}^M(\mathbf{r}) \tag{B.1a}$$

$$= \sum_{L,M} \tilde{a}_{LM}^E \mathbf{E}_{LM}^{E(j')}(\mathbf{r}') + \tilde{a}_{LM}^M \mathbf{E}_{LM}^{M(j')}(\mathbf{r}'). \tag{B.1b}$$

Noting the relations [35]

$$\mathbf{E}_{lm}^{E(j)}(\mathbf{r}) = \sum_{L,M} \mathcal{A}_{LM}^{lm(j'')}(\mathbf{r}_{\mathrm{NP}})\mathbf{E}_{LM}^{E(j')}(\mathbf{r}') + \frac{k}{k_2}\mathcal{B}_{LM}^{lm(j'')}(\mathbf{r}_{\mathrm{NP}})\mathbf{E}_{LM}^{M(j')}(\mathbf{r}'), \tag{B.2a}$$

$$\mathbf{E}_{lm}^{M(j)}(\mathbf{r}) = \sum_{L,M} \mathcal{A}_{LM}^{lm(j'')}(\mathbf{r}_{\mathrm{NP}})\mathbf{E}_{LM}^{M(j')}(\mathbf{r}') + \frac{k_2}{k}\mathcal{B}_{LM}^{lm(j'')}(\mathbf{r}_{\mathrm{NP}})\mathbf{E}_{LM}^{E(j')}(\mathbf{r}') \tag{B.2b}$$

yields

$$\tilde{a}^E_{LM} = \sum_{l,m} a^E_{lm} \mathcal{A}^{lm(j'')}_{LM}(\mathbf{r}_{\rm NP}) + \frac{k_2}{k} a^M_{lm} \mathcal{B}^{lm(j'')}_{LM}(\mathbf{r}_{\rm NP}), \tag{B.3a}$$

$$\tilde{a}^M_{LM} = \sum_{l,m} a^M_{lm} \mathcal{A}^{lm(j'')}_{LM}(\mathbf{r}_{\rm NP}) + \frac{k}{k_2} a^E_{lm} \mathcal{B}^{lm(j'')}_{LM}(\mathbf{r}_{\rm NP}), \tag{B.3b}$$

where explicit expressions for the shift coefficients $\mathcal{A}^{lm(j'')}_{LM}(\mathbf{r}_{\rm NP})$ and $\mathcal{B}^{lm(j'')}_{LM}(\mathbf{r}_{\rm NP})$ can be found in the work of Xu [56]. Care, however, must be taken with regards to the normalization of the Mie modes, and the resulting scaling of the shift coefficients. Specifically, in this work an additional factor of $\sqrt{[(2l+1)(L+M)!(l-m)!]/[(2L+1)(L-M)(l+m)!]}$, is introduced into equations (75) and (76) of Xu's work [56].

In this paper a dipole approximation is often made for the scatterer NP, such that only $\mathcal{A}^{1m(j'')}_{lm} = \mathcal{A}^{1m(j'')}_{lm}(\mathbf{r}_{\rm NP})$ and $\tilde{\mathcal{A}}^{lm(j'')}_{1m} = \mathcal{A}^{lm(j'')}_{1m}(-\mathbf{r}_{\rm NP})$ (and similarly for $\mathcal{B}^{1m(j'')}_{lm}(\mathbf{r}_{\rm NP})$ and $\mathcal{B}^{lm(j'')}_{1m}(-\mathbf{r}_{\rm NP})$) need to be considered. It can then be shown that

$$\begin{bmatrix} \tilde{\mathcal{A}}^{lm(j'')}_{1m} \\ \tilde{\mathcal{B}}^{lm(j'')}_{1m} \end{bmatrix} = \frac{2}{l(l+1)} \begin{bmatrix} \mathcal{A}^{1m(j'')}_{lm} \\ -\mathcal{B}^{1m(j'')}_{lm} \end{bmatrix}, \tag{B.4}$$

where

$$\mathcal{A}^{1m(j'')}_{lm} = \frac{l(l+1)}{2(1+m)!} \left[\frac{3}{(2l+1)} \frac{(l-m)!}{(1-m)!} \frac{(1+m)!}{(l+m)!} \right]^{1/2} \left[\frac{(l+m)!}{l!} h^{(j'')}_{l-1}(kr_{\rm NP}) + \frac{(-1)^m\, l!}{(l-m)!} h^{(j'')}_{l+1}(kr_{\rm NP}) \right] \tag{B.5}$$

and

$$\mathcal{B}^{1m(j'')}_{lm} = \frac{\mathrm{i}m}{2} \left[\frac{3}{(2l+1)} \frac{(l-m)!}{(1-m)!} \frac{(l+m)!}{(1+m)!} \right]^{1/2} \frac{(2l+1)}{(l-1)!} h^{(j'')}_{l}(kr_{\rm NP}). \tag{B.6}$$

The correct choice of j' and j'' is dependant on the position at which the field is to be evaluated. Specifically it is noted that $j' = 3$, $j'' = j$ for $r' < r_{\rm NP}$ and $j' = j$, $j'' = 3$ for $r' \geqslant r_{\rm NP}$.

Appendix C. Scaling parameter for a core–shell nanoparticle

The mode coefficients for the field scattered from a core–shell NP are given (analogously to equation (3c)) by $\tilde{d}^{\nu}_{lm} = \kappa^{\nu}_l(k^{\rm I}, k^{\rm III}, k^{IV}, r_{\rm III}, r_{\rm IV})\tilde{b}^{\nu}_{lm}$ where $k_{\rm III}$ and $k_{\rm IV}$ denote the wavenumber in the shell and core regions respectively, which have radii $r_{\rm III}$ and $r_{\rm IV}$ (see figure 5). Using the shorthand notation $z^i_j = k^i r_j$ and letting $\kappa^{\nu,2}_l = \kappa^{\nu}_l(k^{\rm I}, k^{\rm III}, k^{IV}, r_{\rm III}, r_{\rm IV})$ it is possible to show

$$\kappa^{\nu,2}_l = \frac{k^{\rm I}_s \Phi^{\nu}_l(z^{\rm III}_{\rm III}) h^{(3)}_l(z^{\rm I}_{\rm III}) - k^{\rm III}_s H^{\nu}_l(z^{\rm III}_{\rm III}) \psi^{(3)}_l(z^{\rm I}_{\rm III})}{k^{\rm III}_s H^{\nu}_l(z^{\rm III}_{\rm III}) \psi^{(1)}_l(z^{\rm I}_{\rm III}) - k^{\rm I}_s \Phi^{\nu}_l(z^{\rm III}_{\rm III}) h^{(1)}_l(z^{\rm I}_{\rm III})} \tag{C.1}$$

with $s = 1$ or 2 for $\nu = E$ or M respectively, where

$$\Phi^{\nu}_l(z) = \psi^{(2)}_l(z)\tau^{\nu,2}_l + \psi^{(1)}_l(z)\mu^{\nu,2}_l, \tag{C.2a}$$

$$H^{\nu}_l(z) = h^{(2)}_l(z)\tau^{\nu,2}_l + h^{(1)}_l(z)\mu^{\nu,2}_l \tag{C.2b}$$

and

$$\tau_l^{v,2} = \frac{k_s^{\mathrm{IV}}\psi_l^{(1)}(z_{\mathrm{IV}}^{\mathrm{III}})h_l^{(3)}(z_{\mathrm{IV}}^{\mathrm{IV}}) - k_s^{\mathrm{III}}h_l^{(1)}(z_{\mathrm{IV}}^{\mathrm{III}})\psi_l^{(3)}(z_{\mathrm{IV}}^{\mathrm{IV}})}{k_s^{\mathrm{III}}h_l^{(2)}(z_{\mathrm{IV}}^{\mathrm{III}})\psi_l^{(1)}(z_{\mathrm{IV}}^{\mathrm{III}}) - k_s^{\mathrm{III}}\psi_l^{(2)}(z_{\mathrm{IV}}^{\mathrm{III}})h_l^{(1)}(z_{\mathrm{IV}}^{\mathrm{III}})}, \tag{C.3a}$$

$$\mu_l^{v,2} = \frac{k_s^{\mathrm{III}}\psi_l^{(3)}(z_{\mathrm{IV}}^{\mathrm{IV}})h_l^{(2)}(z_{\mathrm{IV}}^{\mathrm{III}}) - k_s^{\mathrm{IV}}h_l^{(3)}(z_{\mathrm{IV}}^{\mathrm{IV}})\psi_l^{(2)}(z_{\mathrm{IV}}^{\mathrm{III}})}{k_s^{\mathrm{III}}h_l^{(2)}(z_{\mathrm{IV}}^{\mathrm{III}})\psi_l^{(1)}(z_{\mathrm{IV}}^{\mathrm{III}}) - k_s^{\mathrm{III}}\psi_l^{(2)}(z_{\mathrm{IV}}^{\mathrm{III}})h_l^{(1)}(z_{\mathrm{IV}}^{\mathrm{III}})}. \tag{C.3b}$$

Appendix D. Derivation of equation (23)

To derive equation (23) it is sufficient to start from equation (5) (with omission of the m subscript as described in section 2), whereby some minor rearrangement yields

$$\begin{bmatrix}\mathbf{b}^E\\ \mathbf{b}^M\end{bmatrix} = \begin{bmatrix}\mathbb{N}^{E,1} & \mathbb{0}\\ \mathbb{0} & \mathbb{N}^{M,1}\end{bmatrix}\left\{\begin{bmatrix}\mathbf{a}^E\\ \mathbf{a}^M\end{bmatrix} + \begin{bmatrix}\mathbb{\Delta}_1 & \mathbb{\Delta}_3\\ \mathbb{\Delta}_4 & \mathbb{\Delta}_2\end{bmatrix}\begin{bmatrix}\mathbf{b}^E\\ \mathbf{b}^M\end{bmatrix}\right\}$$

which can be more concisely written as

$$\mathbf{b} = \mathbb{N}(\mathbf{a} + \mathbb{\Delta}\mathbf{b}). \tag{D.1}$$

Left multiplying by $\mathbb{\Delta}$ and collecting terms subsequently gives $\mathbb{\Delta}\mathbf{b} = [\mathbb{I} - \mathbb{\Delta}\mathbb{N}]^{-1}\,\mathbb{\Delta}\mathbb{N}\mathbf{a}$, which upon back substitution into equation (D.1) yields

$$\mathbf{b} = \mathbb{N}(\mathbf{a} + [\mathbb{I} - \mathbb{\Delta}\mathbb{N}]^{-1}\,\mathbb{\Delta}\mathbb{N}\mathbf{a}). \tag{D.2}$$

If the off diagonal blocks of $\mathbb{\Delta}$ (i.e. $\mathbb{\Delta}_3$ and $\mathbb{\Delta}_4$) are neglected equation (D.2) is block diagonal allowing separation into two independent matrix equations, namely those specified by equation (23).

References

[1] Giannini V, Fernández-Domínguez A I, Heck S C and Maier S A 2011 Plasmonic nanoantennas: fundamentals and their use in controlling the radiative properties of nanoemitters *Chem. Rev.* **111** 3888–912

[2] Lal S, Link S and Halas N J 2007 Nano-optics from sensing to waveguiding *Nature Photon.* **1** 3641–48

[3] Maier S 2007 *Plasmonics: Fundamentals and Applications* (Berlin: Springer)

[4] Homola J 2008 Surface plasmon resonance sensors for detection of chemical and biological species *Chem. Rev.* **108** 462–93

[5] Homola J 2006 *Surface Plasmon Resonance Based Sensors* (*Springer Series on Chemical Sensors and Biosensors* vol 4) (Berlin: Springer)

[6] Min B, Ostby E, Sorger V, Ulin-Avila E, Yang L, Zhang X and Vahala K 2009 High-Q surface-plasmon-polariton whispering-gallery microcavity *Nature* **457** 455–8

[7] Anker J N, Hall W P, Lyandres O, Shah N C, Zhao J and Van Duyne R P 2008 Biosensing with plasmonic nanosensors *Nature Mater.* **7** 442–53

[8] Mayer K M and Hafner J H 2011 Localized surface plasmon resonance sensors *Chem. Rev.* **111** 3828–57

[9] Baaske M and Vollmer F 2012 Optical resonator biosensors: molecular diagnostic and nanoparticle detection on an integrated platform *Chem. Phys. Chem.* **13** 427–36

[10] Gorodetsky M L, Savchenkov A A and Ilchenko V S 1996 Ultimate Q of optical microsphere resonators *Opt. Lett.* **21** 453–5

[11] Vollmer F, Arnold S and Keng D 2008 Single virus detection from the reactive shift of a whispering-gallery mode *Proc. Natl Acad. Sci. USA* **105** 20701–4

[12] Arnold S, Keng D, Shopova S, Holler S, Zurawsky W and Vollmer F 2009 Whispering gallery mode carousel—a photonic mechanism for enhanced nanoparticle detection in biosensing *Opt. Express* **17** 6230–8
[13] Waldron R A 1960 Perturbation theory of resonant cavities *Proc. Inst. Electr. Eng.* **107C** 272–4
[14] Klein O, Ponova S, Dressel M and Greiner G 1993 Microwave cavity perturbation technique: I. Principles *Int. J. Infrared Millim. Waves* **14** 2423–57
[15] Arnold S, Khoshsima M, Teraoka I, Holler S and Vollmer F 2003 Shift of whispering-gallery modes in microspheres by protein adsorption *Opt. Lett.* **28** 272–4
[16] Teraoka I, Arnold S and Vollmer F 2003 Perturbation approach to resonance shifts of whispering-gallery modes in a dielectric microsphere as a probe of a surrounding medium *J. Opt. Soc. Am.* B **20** 1937–46
[17] Teraoka I and Arnold S 2006 Theory of resonance shifts in TE and TM whispering gallery modes by non-radial perturbations for sensing applications *J. Opt. Soc. Am.* B **23** 1381–9
[18] Shopova S I, Rajmangal R, Holler S and Arnold S 2011 Plasmonic enhancement of a whispering-gallery-mode biosensor for single nanoparticle detection *Appl. Phys. Lett.* **98** 243104
[19] Xiao Y-F, Liu Y-C, Li B-B, Chen Y-L, Li Y and Gong Q 2012 Strongly enhanced light–matter interaction in a hybrid photonic–plasmonic resonator *Phys. Rev.* A **85** 031805
[20] Dantham V R, Holler S, Kolchenko V, Wan Z and Arnold S 2012 Taking whispering gallery-mode single virus detection and sizing to the limit *Appl. Phys. Lett.* **101** 043704
[21] Arnold S, Dantham V R, Barbre C, Garetz B A and Fan X 2012 Periodic plasmonic enhancing epitopes on a whispering gallery mode biosensor *Opt. Express* **20** 26147–60
[22] Santiago-Cordoba M A, Cetinkaya M, Boriskina S V, Vollmer F and Demirel M C 2012 Ultrasensitive detection of a protein by optical trapping in a photonic–plasmonic microcavity *J. Biophoton.* **10** 1–10
[23] Lin S and Crozier K B 2013 Trapping-assisted sensing of particles and proteins using on-chip optical microcavities *ACS Nano* **7** 1725–30
[24] Santiago-Cordoba M A, Boriskina S V, Vollmer F and Demirel M C 2011 Nanoparticle-based protein detection by optical shift of a resonant microcavity *Appl. Phys. Lett.* **99** 073701
[25] Witzens J and Hochberg M 2011 Optical detection of target molecule induced aggregation of nanoparticles by means of high-Q resonators *Opt. Express* **19** 7034–61
[26] Dantham V R, Holler S, Kolchenko V, Wan Z and Arnold S 2013 Microcavity single virus detection and sizing with molecular sensitivity *Proc. SPIE* **8600** 86001P
[27] Hao E and Schatz G C 2004 Electromagnetic fields around silver nanoparticles and dimers *J. Chem. Phys.* **120** 357–66
[28] Weiss D S, Sandoghdar V, Hare J, Lefèvre-Seguin V, Raimond J M and Haroche S 1995 Splitting of high-Q Mie modes induced by light backscattering in silica microspheres *Opt. Lett.* **20** 1835–7
[29] Deych L and Rubin J 2009 Rayleigh scattering of whispering gallery modes of microspheres due to a single dipole scatterer *Phys. Rev.* A **80** 061805
[30] Waterman P C 1969 New formulation of acoustic scattering *J. Acoust. Soc. Am.* **45** 1417–29
[31] Gouesbet G and Grehan G 1999 Generalized Lorenz–Mie theory for assemblies of spheres and aggregates *J. Opt. A: Pure Appl. Opt.* **1** 706–71
[32] Vollmer F and Arnold S 2008 Whispering-gallery-mode biosensing: label-free detection down to single molecules *Nature Methods* **5** 591–6
[33] Deych L, Schmidt S, Chipouline A, Pertsch T and Tünnermann A 2008 Optical coupling of fundamental whispering-gallery modes in bispheres *Phys. Rev.* A **77** 051801
[34] Mishchenko M I 2000 Calculation of the amplitude matrix for a nonspherical particle in a fixed orientation *Appl. Opt.* **39** 1026–31
[35] Mishchenko M I, Travis L D and Lacis A A 2002 *Scattering, Absorption and Emission of Light by Small Particles* (Cambridge: Cambridge University Press)
[36] Moroz A 2005 Improvement of Mishchenko's T matrix code for absorbing particles *Appl. Opt.* **44** 3605–9
[37] Bohren C F and Huffman D R 1998 *Absorption and Scattering of Light by Small Particles* (Weinheim: Wiley)

[38] van de Hulst H C 1981 *Light Scattering by Small Particles* (Mineola, NY: Dover Publications)
[39] Gasiorowicz S 2003 *Quantum Physics* 3rd edn (New York: Wiley)
[40] Rubin J T and Deych L 2010 *Ab initio* theory of defect scattering in spherical whispering-gallery-mode resonators *Phys. Rev.* A **81** 053827
[41] Halas N 2002 The optical properties of nanoshells *Opt. Photon. News* **13** 26–30
[42] Huang H, Yu C, Chang H, Chiu K, Ming H Chen, Liu R and Tsai D 2007 Plasmonic optical properties of a single gold nano-rod *Opt. Express* **15** 7132–9
[43] Zhou Z-K, Peng X-N, Yang Z-J, Zhang Z-S, Li M, Su X-R, Zhang Q, Shan X, Wang Q-Q and Zhang Z 2011 Tuning gold nanorod–nanoparticle hybrids into plasmonic Fano resonance for dramatically enhanced light emission and transmission *Nano. Lett.* **11** 49–55
[44] Mackowski D W, Altenkirch R A and Menguc M P 1990 Internal absorption cross sections in a stratified sphere *Appl. Opt.* **29** 1551–9
[45] Mackowski D W 1991 Analysis of radiative scattering for multiple sphere configurations *Proc. R. Soc. Lond.* A **433** 599–614
[46] Teraoka I and Arnold S 2009 Resonance shifts of counter-propagating whispering-gallery modes: degenerate perturbation with axial symmetry *J. Opt. Soc. Am.* B **26** 1321–9
[47] Johnson B R 1993 Theory of morphology-dependent resonances: shape resonances and width formulas *J. Opt. Soc. Am.* A **10** 343–52
[48] Schiller S 1993 Asymptotic expansion of morphological resonance frequencies in Mie scattering *Appl. Opt.* **32** 2181–5
[49] Lam C C, Leung P T and Young K 1992 Explicit asymptotic formulas for the positions, widths and strengths of resonances in Mie scattering *J. Opt. Soc. Am.* B **9** 1585–92
[50] Kreibig U 1974 Electronic properties of small silver particles: the optical constants and their temperature dependence *J. Phys. F: Metal Phys.* **4** 999–1014
[51] Miao X, Brener I and Luk T S 2010 Nanocomposite plasmonic fluorescence emitters with core/shell configurations *Opt. J. Soc. Am.* B **27** 1561–70
[52] Foreman M R and Vollmer F 2013 Level repulsion in hybrid photonic–plasmonic microresonators for enhanced biodetection, in preparation
[53] Novotny L 2010 Strong coupling, energy splitting and level crossings: a classical perspective *Am. J. Phys.* **78** 1199–201
[54] Foreman M R, Sivan Y, Maier S A and Török P 2012 Independence of plasmonic near-field enhancements to illumination beam profile *Phys. Rev.* B **86** 155441
[55] Born M and Wolf E 1980 *Principles of Optics* 7th edn (Cambridge: Cambridge University Press)
[56] Xu Y-L 1996 Calculation of the addition coefficients in electromagnetic multisphere-scattering theory *J. Comput. Phys.* **127** 285–98